Chapter 5
Morphology Development and Control

Roberto Pantani, Felice De Santis and Vito Speranza

Contents

R. Pantani (✉) · V. Speranza
Department of Industrial Engineering, University of Salerno, Fisciano, SA, Italy
e-mail: rpantani@unisa.it

V. Speranza
e-mail: vsperanza@unisa.it

F. De Santis
Borealis Polyolefine GmbH, Linz, Austria
e-mail: fedesantis@unisa.it

J. Karger-Kocsis and T. Bárány (eds.), *Polypropylene Handbook*,
https://doi.org/10.1007/978-3-030-12903-3_5

Abstract When referred to polymers, the word morphology is adopted to indicate: crystallinity, which is the relative volume occupied by each of the crystalline phases, including mesophases; dimensions, shape, distribution, and orientation of the crystallites. In this chapter, we describe the morphology of isotactic polypropylene in function of the main variables: temperature, pressure, and flow. This description is carried out not only under the phenomenological point of view but also considering the models which describe the effects of these variables. The chapter describes then the morphology development during injection molding, which is taken as an example of a complex process in which fast cooling rates, high pressures and strong flow fields are involved. A case study in which the simulation of the behavior of polypropylene during injection molding tests is eventually reported.

5.1 Introduction

The properties of polypropylene (PP) depend on the molecular weight and molecular weight distribution, crystallinity, type and proportion of comonomer (if used) and the isotacticity. In isotactic polypropylene, for example, the methyl groups are oriented on one side of the carbon backbone. This arrangement creates a greater degree of crystallinity, of about 60%, and results in a stiffer material that is more resistant to creep than both atactic polypropylene and polyethylene.

Most commercial and important polypropylene is isotactic, and thus in this chapter from here on it will be referred to polypropylene without mentioning "isotactic".

This chapter will deal in particular with the morphology of polypropylene. The term *morphology* means "the study of the form" where form stands for the shape and arrangement of parts of the object. When referred to polymers, the word morphology is adopted to indicate the following:

- crystallinity, which is the relative volume occupied by each of the crystalline phases, including mesophases;
- dimensions, shape, distribution, and orientation of the crystallites.

The variety of plastic characteristics (mechanical, optical, electrical, transport, and chemical) derives not only from the chemical structure of molecules but also from the microstructure and morphology. For instance, crystallinity has a pronounced effect on the mechanical properties of the bulk material because crystals are generally stiffer than amorphous material, and also orientation induces anisotropy and other changes in mechanical properties. Molecular orientation, or simply orientation, arises in injection molding and may have desirable or undesirable consequences. It refers to the preferential alignment of macromolecules in the product. Tensile strength in the orientation direction is basically that of the carbon–carbon (or other covalent bonds) in the polymer backbone. In the transverse direction, the strength is provided by the secondary intramolecular bonds. Hence, uniaxially oriented materials will be much stronger and stiffer in one direction than in another.

The production of high quality polymeric parts, which is a sector in great expansion, requires the capacity of being able to predict and control these morphological features.

In this chapter, the state of the art on the effect of the main processing variables on the formation of the crystalline phases and on the morphology of isotactic polypropylene is carried out, with particular reference to injection molding. This particular process is taken as a reference in this chapter because in injection molding the contemporary effects of high pressures, strong flow fields, and fast cooling rates allow the development of several crystalline phases and structures, unique in all the polymer transformation techniques. The effect of other processing techniques on morphology evolution are briefly outlined at the end of the chapter.

5.1.1 Characteristics of Polypropylene

Isotactic polypropylene can crystallize in different phases. The most common phase is α [1], which is formed at low pressures and at low cooling rates [2]. In the presence of specific nucleating agents, or of specific flow conditions, β-phase can develop [3]. At high pressures and temperatures, γ-phase is formed [4] (see Chap. 2 of this book). A mesomorphic phase is formed at cooling rates higher than 100 K/s [5]. The presence of each of these phases induces different properties to the parts made of polypropylene. The α phase makes polypropylene rigid and strong. In contrast, β phase induces a lower modulus and yield stress, but higher tensile strength and strain, impact strength and toughness [6]. The γ phase has been reported to induce higher elastic modulus and yield stress with respect to α phase, but a slightly lower ultimate strain [7]. A large amount of mesophase makes the material ductile and flexible [8], and also reduces the density [2].

Apart from the phases, polypropylene can crystallize in different shapes. Spherulitic structures appear when the material crystallizes in quiescent conditions, as a result of nucleation and growth phenomena. The size of the spherulites affects the mechanical [9] and optical properties [10] with a general increase of impact strength and transparency on decreasing the spherulite size. In samples containing both phases, β spherulites are usually larger than α spherulites. Under flow conditions, polymer chains are oriented in the melt and can crystallize differently from quiescent conditions. For example, by the effect of flow, the so-called "shish-kebabs" can be formed [11] (see Chap. 4 of this book). In these structures a highly oriented core composed of extended chains ("shish") forms, on which oriented chain folded lamellae ("kebabs") grow. These structures usually induce larger moduli and strain at break if deformed in the direction of main orientation [12].

What stated above provides a clear indication that the properties of an object made of polypropylene depends upon the particular crystalline phase and on the structures obtained. The prediction of the final morphology in function of the processing conditions and, above all, the control of the morphological features, is a strategic issue for the polymer processing industry.

5.1.2 Processing of PP

About 40% of polypropylene consumption is processed by injection molding. A lower amount (about 30%) is processed for obtaining fibers by means of fiber spinning. About 20% is the quota used for films. Other processes, like blow molding, represent minor transformation techniques for this material.

As far as morphology development is concerned, cooling rates, deformation fields, and pressure levels play a role during processing [13]. Under this aspect, the main differences between injection molding and other processes like fiber spinning or film blowing rely: on the type of deformation, which is basically due to shear in injection molding (except in narrow sections in which elongational flow can be significant), whereas it is uniaxial in fiber spinning and biaxial in film blowing; on the effect of pressure, since in injection molding the pressure can reach several hundreds of bar, whereas pressure is atmospheric in other processes.

It is evident that injection molding is the processing technique which presents the most complete set of conditions under which morphology development takes place. This is the reason why in the following we refer mainly to this process for the description of morphology evolution of polypropylene in processing conditions.

5.2 Crystallization Kinetics of PP

Traditional studies of polymer crystallization kinetics started from idealized conditions in which all parameters of state (temperature, pressure, etc.) are constants. The importance of crystallization kinetics of polypropylene during industrial processing obviously led to investigate the influence of variable external conditions.

5.2.1 Effect of Temperature

The early models of crystallization in variable conditions concerned only variation of temperature. Standard calorimetric characterization (adopting both isothermal and non-isothermal tests) was performed by means of a Differential Scanning Calorimetry (DSC) apparatus. The thermal inertia of the standard calorimetric cells limited the exploration range for isotactic polypropylene to heating/cooling rate of less than 1 K/s. In fact, PP is considered a fast crystallizing polymer, because of the simple macromolecular chain,

Furthermore, some corrections were proposed to take into account the low heat transfer coefficient of the polymer, according to the procedure illustrated by Eder and Janeschitz-Kriegl [13].

For the same reason, the explored range using DSC in isothermal conditions is limited by the maximum attainable cooling rate, able to prevail crystallization before reaching isothermal test temperature.

In order to describe PP crystallinity evolution under high cooling rates, usually experienced in processing conditions, many efforts have been spent along this direction. In particular, the effect of high cooling rates was analyzed in a series of works conducted by Piccarolo et al. [14] and Coccorullo et al. [2], in which the morphology of samples solidified under high cooling rates (hundreds of K/s) was investigated, observing the formation of a mesophase. Magill [15] and Ding et al. [16] measured crystallinity evolution during cooling at moderate cooling rates (up to about 3 K/s) by means of optical methods. This approach was extended by Titomanlio and co-workers to higher cooling rates (30 K/s) [17, 18].

Modulus, ductility, and strength can be modulated through the crystallization of α phase or the mesophase. Different morphologies are observed depending on the stereoregularity and conditions of crystallization [5]. Crystals of the mesomorphic form always exhibit a nodular morphology, accounting for the similar good deformability of all quenched samples. The mesophase transforms by thermal treatments (annealing at elevated temperature) into the α form preserving the nodular morphology, with an increase of strength while maintaining the ductility typical of the mesophase as shown in Fig. 5.1. Annealing of the mesophase permits

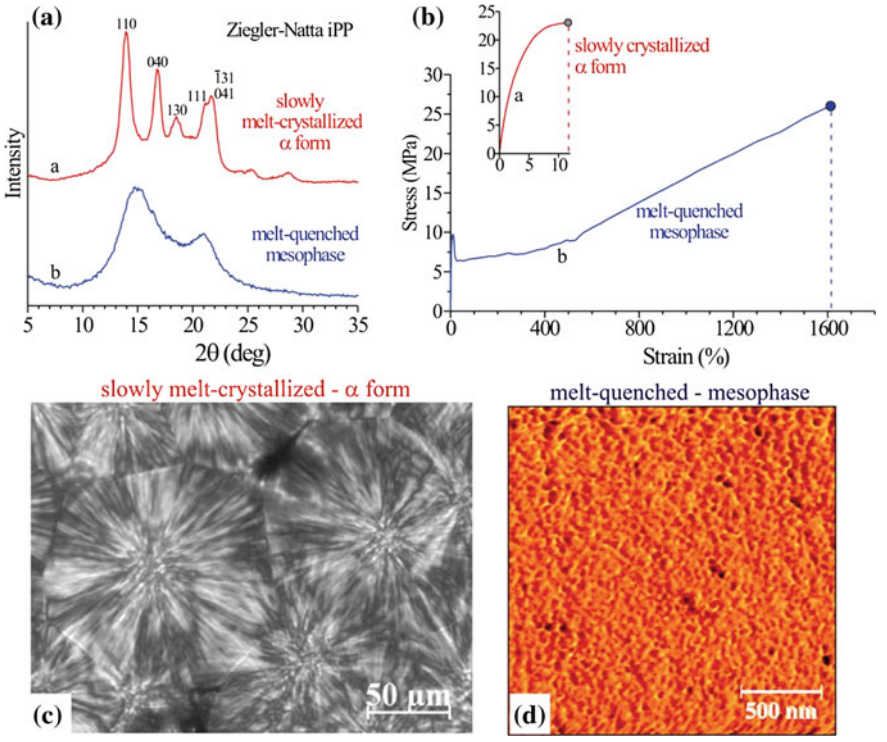

Fig. 5.1 X-ray powder diffraction profiles (**a**), stress–strain curves (**b**) and optical microscopy (**c**) and AFM (**d**) images of samples of highly stereoregular iPP slowly crystallized from the melt in the α form (**a**) and crystallized in the mesophase by quenching the melt at 0 °C (**b**). Reproduced from [5]

a precise adjustment of crystallinity and size of nodular crystals offering additional options to modify the mechanical properties.

More recently the introduction of nanocalorimetry performed with Flash DSC [19] opened the possibility to further explore the crystallization kinetics of PP. In particular, a wide set of cooling scans and subsequent melting behavior of PP were investigated using Flash DSC at very high cooling rate. This technique offered the possibility to perform calorimetric measurements at rates of more than 1000 K/s, both in cooling and in heating, to characterize the crystallization. As shown in Fig. 5.2, when the iPP sample was solidified with cooling rate larger than 160 K/s, a novel enthalpic process was observed that was related to the mesomorphic phase formation [20]. Furthermore, at cooling rates higher than 1000 K/s, the PP sample did not crystallize in the α or in the mesomorphic form. The subsequent heating scan starting from −15 °C showed an exothermic event, between 0 and 30 °C, attributed to the mesophase cold crystallization [20].

Therefore a wide set of crystallization isotherms and the subsequent melting behavior of isotactic polypropylene were investigated using Flash DSC with a very high rate in the cooling step [21]. Isothermal crystallization experiments were carried at any temperature in between the glass transition and melting, as the test temperature can be reached at a cooling rate of 1000 K/s, thus, preventing crystallization during the cooling step. Isothermal tests after such fast cooling were performed at intervals of 5 K within the temperature range −15–90 °C, and a local exothermal overheating was observed, as shown in Fig. 5.3.

In particular, for each isotherm, the observed peaks were fitted using the Kolmogorov − Johnson − Mehl − Avrami model. The plot of the crystallization kinetics constant as a function of temperature gives clear evidence of two kinetic processes [21], related to α and mesomorphic phases. The subsequent heating scan

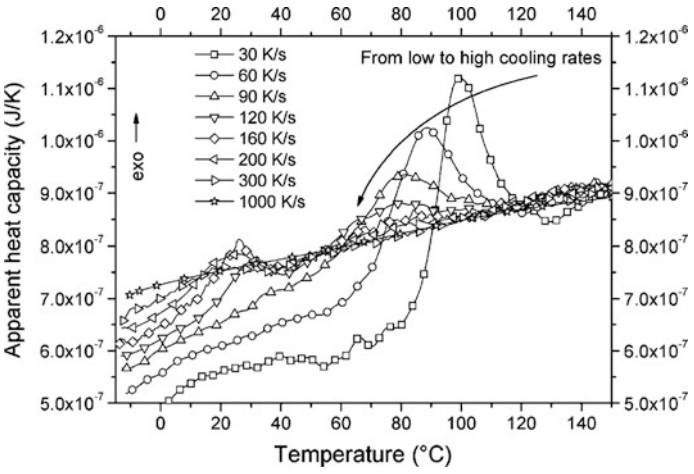

Fig. 5.2 Thermograms of iPP sample at selected cooling rates (30, 60, 90, 120, 160, 200, 300, and 1000 K/s). Reproduced from [20]

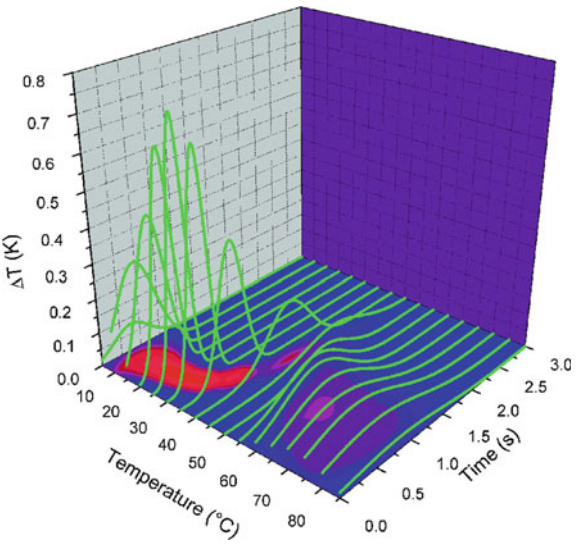

Fig. 5.3 Temperature increase evolution versus time for each isothermal test. Reproduced from [21].

performed starting from −15 °C showed an exothermic event, between 0 and 30 °C, due to the mesophase cold crystallization, for isotherms at a temperature lower than 20 °C.

The result of the kinetic analysis, i.e. the reciprocal crystallization rate constant k, proportional to crystallization half-time, is reported in Fig. 5.4. The same plot also shows a large number of kinetic data available in the literature concerning the isothermal crystallization of iPP [21], obtained from experiments collected with various methods. Despite the scatter due to the experiments performed on different iPP resins, the results, plotted in Fig. 5.4, clearly indicate a focused band from 110–160 °C. The kinetic data, obtained by interpreting nanocalorimetry isothermal results [21], covered a range of temperatures from 5–85 °C, mostly unexplored previously. In Fig. 5.4, it is evident that at temperatures lower than 45 °C, there is a variation in the kinetic behavior: the mesophase is formed by homogeneous nucleation (Avrami index n = 4) and above 45 °C, the α phase prevails due to heterogeneous nucleation (Avrami index n = 3) [21].

5.2.2 *Effect of Pressure*

During industrial processing, melt polymers are subjected to high pressure, that has an important influence on the material flowing, solidification, and the final properties. At atmospheric pressure, the γ phase of isotactic polypropylene appears under various conditions, for instance when the polymer chains are short [22] or in the case of a ethylene-propylene copolymer with a small amount of ethylene [23, 24]. However, the main way to obtain γ structure for a high molecular weight

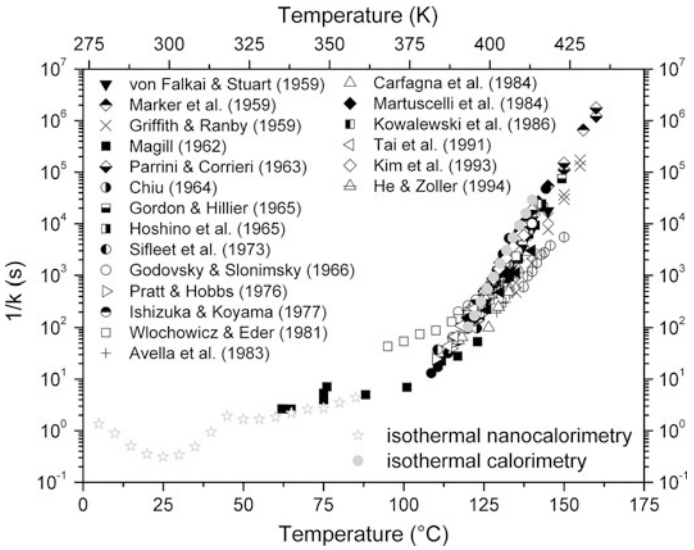

Fig. 5.4 Cumulative data of the isothermal crystallization of iPP: variation of the reciprocal crystallization rate constant k as a function of crystallization temperature. Black symbols: literature data reported in [21]. Isothermal nanocalorimetry and isothermal calorimetry as gray stars and circles, respectively. Reproduced from [21]

homopolymer is to perform crystallization under high pressure [25, 26]. This structure usually become dominant at pressures higher than 200 MPa [27, 28]. The γ form of isotactic polypropylene is certainly the most peculiar considering the nonparallel chain axes, coexisting in the orthorhombic unit cell which was first proposed by Brückner and Meille [25, 29]. Even if, about 50 years ago, it was established that the ratio between the γ-iPP and the α-iPP polymorphs grows with increasing pressure, the solidification process under this conditions still needs to be properly described and quantified [4].

Experimental data, performed in isothermal experiments varying pressure, on the dependence of the specific volume on temperature and pressure, up to 200 MPa, were reported thanks to the High-pressure Dilatometer developed by Zoller [30, 31], as shown in Fig. 5.5.

The specific volume is smaller with increasing pressure, at the same temperature, and the melting transition is evident in Fig. 5.5 with a sharp transition. The melting point rises with pressure. Thus PP can be crystallized at much higher temperatures when pressure is applied. The crystallization under these conditions of high pressures and temperatures has been studied. Zoller et al. [32] explored the pressure effect on crystallization kinetics performing isobaric measurements at constant heating and cooling rate of 2.5 K/min, as shown in Fig. 5.6.

For PP in the semicrystalline region, the volumes in cooling runs are higher than those in heating runs. The volume difference apparently increases with pressure. This indicates that the high pressure crystallization produces samples of lower

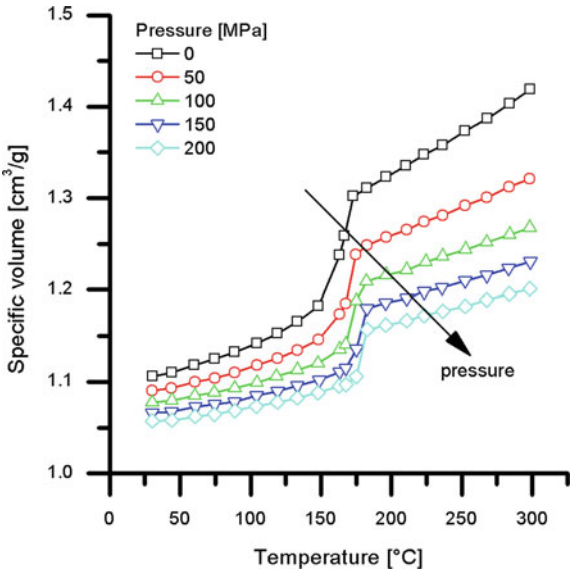

Fig. 5.5 Cross-plotted isobars, obtained from isothermal PVT measurements taken in order of increasing temperature. Data reproduced from [31]

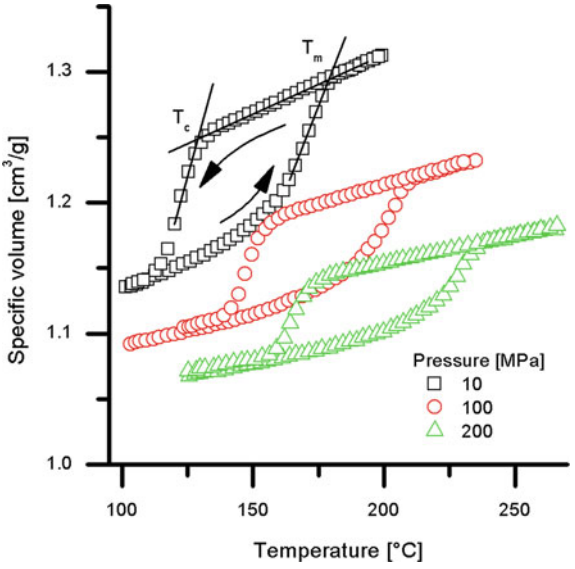

Fig. 5.6 Melting and crystallization isobars of polypropylene at various pressures, with heating and cooling rates: 2.5 K/min. Data reproduced from [32]

density than the low pressure crystallization [32]. The melting and solidification curves are indicated in Fig. 5.6. For all the solidification pressure values, the specific volume in the solid phase at the end of the solidification curve is systematically higher than the one measured at the beginning of the melting curve. This behavior demonstrates that during solidification under pressure some structural transformations occur that can justify the final lower value of density [33].

In particular, He and Zoller [32] explained the reduction of density with the formation of the γ phase, which is less dense than the α phase.

5.2.3 *Effect of Flow*

In the most commonly adopted polymer processes such as extrusion, injection molding, and film blowing, the molten polymer is subjected to intense shear and elongational flow fields. Process conditions deeply affect the resulting microstructure: crystallization kinetics, morphology (size, shape, orientation of crystallites) and presence of different crystalline phases can be dramatically different with respect to reference isothermal, quiescent, and low-pressure conditions, and this can have a strong influence on the final physical properties.

Recent developments in flow-induced crystallization (FIC) have demonstrated the existence of three stages [34] which, for the same polymer at the same temperature and pressure, take place on increasing the flow intensity: (i) the effect of flow upon final morphologies and upon crystallization kinetics is negligible, (ii) the flow causes a strong enhancement of crystallization kinetics but the spherulitic morphology is kept, although the average spherulitic dimension decreases, (iii) the flow deeply influences both morphology and kinetics by causing formation of fibrillar structures in the polymer melt.

The transition from the stage *i* and the stage *ii* takes place on increasing the Weissenberg number, namely the dimensionless product of relaxation time and shear rate. In the stage *ii*, it is generally well accepted that flow affects the crystallization kinetics by increasing the crystallization temperature [35–37]. This enhances the growth rate and the nucleation rate, since at each given temperature the apparent undercooling increases. It was also found [35] that the formation of γ-phase under flow is also due to the increase of undercooling.

A phenomenon which appears in the stage *ii*, not present in stage *i* at least for polypropylene, is the nucleation rate. In fact, nucleation density under quiescent conditions was found constant at a constant temperature, a nucleation rate was observed and measured under steady shear conditions [37]. The nucleation rate was found to increase on increasing the deformation rate (Fig. 5.7a).

Also the growth rate increases on increasing the deformation rate. This phenomenon was ascribed to the apparent undercooling increase due to the increase in the melting temperature. A quantification of the increase in the melting temperature was carried out in the literature [37], as shown in Fig. 5.7b [36], where data of growth rates, collected at 140 °C are reported at different shear rates.

In Fig. 5.7b, the lines passing through the different points refer to a prediction of growth rate carried out by considering the increase of melting temperature (indicated near to each line) in the Hoffman-Lauritzen equation adopted to describe the growth rate.

The transition from the stage *ii* to the stage *iii* takes place with a complete change of structures, with the appearance of so-called shish-kebab. The “shish” are

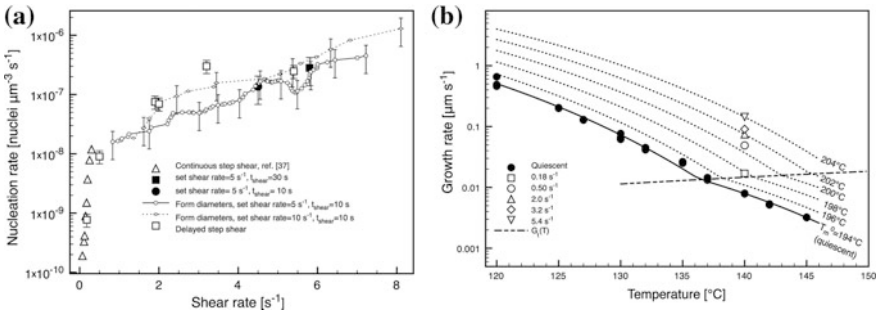

Fig. 5.7 **a** nucleation rate measured from different experiments vs. shear rate; **b** results of growth rate in quiescent conditions (filled circles) and during shear flow. The dashed line identifies the change of growth regime. Predictions of growth rate obtained with different melting temperature are reported as dotted lines. Data reproduced from [36]

fibrillary crystals, whereas the kebabs are radially growing lamellae which nucleate on the shish. Experimental evidence shows that, at each deformation rate, the time required to obtain highly oriented structures decreases with increasing of the deformation rate itself (Fig. 5.8).

The parameter governing this transition is still under debate, with two main hypotheses: a threshold based on a critical Weissenberg number [35], and a threshold based on a critical value of specific work [39, 40]. A more recent approach (described below) proposes a combination of the two criteria.

The shish-kebab morphology presents a complex morphology: kebabs are normally in the stable α-phase, and on their surface, some daughters lamellae can nucleate [41]. These lamellae are still in α-phase and grow at a different angle (40°) with respect to the kebabs. In the presence of pressure, kebab can provide nucleation sites for γ-daughters morphologies [42].

5.2.4 *Effect of Nucleating Agents*

Nucleating agents provide higher polymer crystallization temperatures, creating a larger number of smaller spherulites. The size reduction of spherulites positively affects the optical properties, reducing haze, and may improve flexural modulus and rigidity [43]. The faster crystallization kinetics of nucleated polypropylene also reduces solidification, and thus processing, times. The effects of some nucleating agents on the properties of iPP samples are reported in Fig. 5.9.

Obviously, in order to achieve an optimal efficiency of a nucleating agent, a good dispersion is required. This means that the dispersion techniques are particularly significant.

For polypropylene, nucleating agents can also be used to promote the formation of a specific crystalline phase. A review of advanced nucleating agents can be found

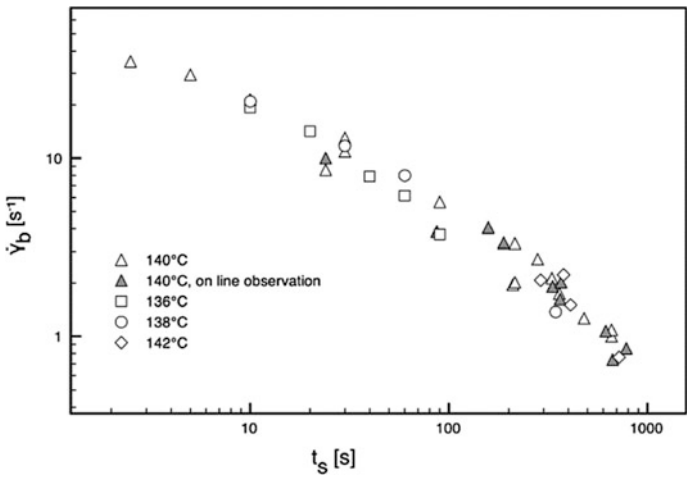

Fig. 5.8 Plot of the critical shear rate at which the oriented structures develop, versus shear time. The temperature at which the tests were conducted is reported. Data reproduced from [38]

in the literature [45]. In Table 5.1 we recall some of the most efficient nucleating agents for the formation of a specific phase in iPP.

It is interesting to notice that the addition of a β-nucleating agent does not affect the rate of mesophase formation at high cooling rates [46], which supports the idea that at high undercooling homogeneous nucleation is the controlling mechanism for ordering.

The efficiency of a nucleating agent is generally estimated by finding the parameter NE% according to the method proposed Fillon et al. [52] (Eq. 5.1):

$$NE\% = 100\frac{T_c - T_{c1}}{T_{c2} - T_{c1}}, \tag{5.1}$$

where T_c, T_{c1} and T_{c2} are peak crystallization temperatures of the nucleated, non-nucleated and self-nucleated polymer, respectively.

The method relies from the assumption that the procedure to determine T_{c2} allows obtaining the highest achievable crystallization temperature. This procedure is based on the following steps, carried out by a DSC apparatus:

- heating the sample to a temperature higher than melting value and maintaining this temperature for 5 min;
- cooling the polymer at a constant cooling rate to room temperature and (during this step the temperature T_{c1} is obtained);
- heating the sample to a temperature at which melting starts, and holding this temperature for 5 min;
- cooling the sample at the same cooling rate that was applied during the second step (during this step the temperature T_{c2} is obtained).

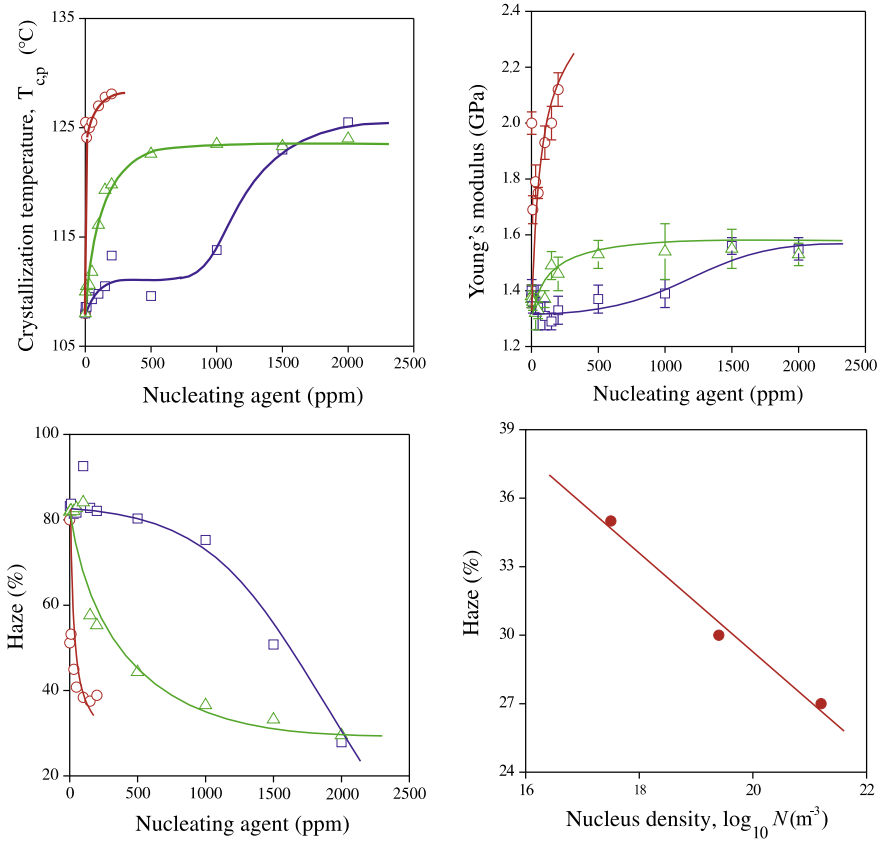

Fig. 5.9 Effect of nucleating agents on the properties of iPP. Circles refer to PVCH, triangles to NA-11, squares to NA21E. Data reproduced from [44]

Table 5.1 Nucleating agents for the formation of a specific phase in iPP

Nucleating agent	Phase	References
PVCH (poly(vinyl cyclohexane))	α	[44]
Na-11 (sodium 2,2′-methylene bis-(4,6-di-tert-butylphenyl)phosphate)	α	[47]
DMDBS (1,3:2,4-bis(3,4-dimethylbenzylidene)-sorbitol)	α	[48]
Linear Trans Quinacridone	β	[49]
Ca-salt of suberic and pimelic acid	β	[49]
N,N'-dicyclohexyl-2,6-naphthalene dicarboxamide	β	[50]
Bicyclo[2.2.1]heptane dicarboxylate salt	γ	[51]

Obviously, much better methods rely on the assessing the crystallization kinetics of the nucleated material [53].

5.2.5 *Effect of Stereo-Defects*

The concentration of stereo-defects, which can be controlled by suitable catalysts, has been found to be able to control the properties of iPP, making it rigid or flexible [5] by inducing the formation of α or γ phases.

In particular, bundle-like elongated crystalline entities and needle-like crystals of γ phase are observed for stereo-irregular samples slowly crystallized from the melt, whereas α phases develops in the same conditions in highly isotactic samples. Stereo-defective samples of iPP crystallize in the mesomorphic phase, regardless of stereoregularity at very high cooling rates. Mesomorphic phase always exhibit a nodular morphology and absence of lamellar spherulitic superstructures, independent of the stereoregularity. This morphology accounts for the similar good deformability of the mesomorphic samples, whatever the concentration of stereo-defects. The mesophase transforms into α phase without affecting the external habit of the crystals, producing α phase with nodular morphology with increase of strength while maintaining the ductility typical of the mesophase [5].

A scheme of the possibilities to tailor ultimate properties of iPP by means of stereo-defects is shown in Fig. 5.10.

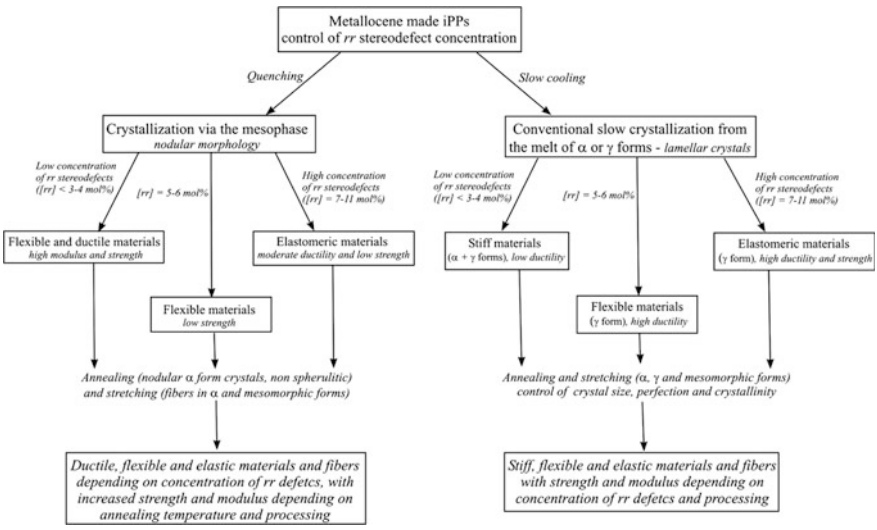

Fig. 5.10 Tailoring of properties of iPP through the control of the concentration of *rr* stereodefects using metallocene catalysts and the crystallization via the mesophase. Reproduced from [5]

5.3 Crystallization Kinetics Models

5.3.1 *Quiescent Crystallization Kinetics*

The evolution of crystallinity in a multiphasic polymer can be described by Eq. 5.2 [54]:

$$\frac{d\xi_i}{dt} = (1 - \xi)\frac{dk_i}{dt}, \tag{5.2}$$

where the subscript "i" stands for α or mesomorphic phase, k_i is the evolution of the undisturbed volume of i-phase, ξ_i is the relative crystallinity degree of i-phase and ξ is the overall relative crystallinity (i.e. the overall volume fraction occupied by crystalline structures and the sum of all the ξ_i).

In the absence of morphological information (such as nucleation and growth rates) the so-called Avrami-Evans-Nakamura kinetic equation (Eq. 5.3) can be used to describe the evolution of the undisturbed volume:

$$\mathrm{k} = ln2\left[\int_0^t K(s)ds\right]^n, \tag{5.3}$$

and the dependence on temperature for the kinetic constant can be described by a simple Gaussian curve (Eq. 5.4):

$$K(T(t)) = K_0 exp\left(-4ln2\frac{(T - T_{\max})^2}{D^2}\right). \tag{5.4}$$

The effect of pressure can be taken into account by considering a linear dependence of T_{max} on pressure (Eq. 5.5):

$$T_{\max} = T_{\max,0} + \alpha_{\max}P. \tag{5.5}$$

This model permits to follow the evolution of the volume occupied by the crystalline structure but does not give details of structure formation, which would, in turn, ignore the effects of the microstructure.

A more detailed model can be used, considering the crystallization kinetics as a sequence of nucleation and growth mechanisms. In this case, Kolmogorov equation can be adopted to describe the evolution of the undisturbed volume (Eq. 5.6).

$$\mathrm{k} = \frac{4\pi}{3}\int_0^t \frac{dN(s)}{ds}\left[\int_s^t G(u)du\right]^3 ds \tag{5.6}$$

$G(T(t))$ is the crystal linear growth rate; and $N(T(t))$ is the nucleation density.

The linear growth rate of crystals can be represented by the Hoffman–Lauritzen expression (Eq. 5.7):

$$G(T(t)) = G_0 \exp\left(-\frac{U}{R(T-T_\infty)}\right)\exp\left(-\frac{K_g(T+T_m)}{2T^2(T_m-T)}\right), \tag{5.7}$$

where G_0 and K_g are parameters and have different values corresponding to different crystallization regimes. Very often the crystallization occurs during the process at lower temperature and therefore only one regime (namely Regime III) has to be considered in the modeling.

The model for describing the nucleation density assumed heterogeneous nucleation, with a number of nuclei depending on temperature according to the Eq. 5.8.

$$N(T(t)) = \frac{N_0}{(1+A_n\exp(B_n(T-T_m))} \tag{5.8}$$

The effect of pressure on N and G can be also considered through the change in the characteristic temperatures, as described in Eq. 5.9.

$$\begin{aligned} T_m &= T_{m,0} + \alpha_m P \\ T_\infty &= T_{\infty,0} + \alpha_\infty P \end{aligned} \tag{5.9}$$

As stated above with Kolmogorov's model, it is possible to describe evolutions of microstructures. In particular, the number of active nuclei at the end of crystallization process can be calculated as (Eq. 5.10):

$$N_{a,final} = \int_a^{t_{final}} \frac{dN[T(s)]}{ds}(1-\xi(s))ds, \tag{5.10}$$

and the average dimension, $\bar{D}$, of crystalline structures can be calculated by geometrical considerations as (Eq. 5.11):

$$\bar{D} = \sqrt[3]{\frac{6\xi_{\alpha,final}}{\pi N_{a,final}}}. \tag{5.11}$$

The radial growth rate, combined with the rate constant, can be used to evaluate the nuclei density as a function of temperature [55]. If crystal growth is assumed to be three-dimensionally spherulitic, the Avrami exponent is n = 3 and the nuclei density, N, at a given temperature, takes the form [55, 56] (Eq. 5.12):

$$N(T) = \frac{3\ln(2)\xi_\infty}{4\pi}\left[\frac{K(T)}{G(T)}\right]^3, \tag{5.12}$$

in which ξ_∞ is the final volume fraction occupied by spherulitic structures.

5.3.2 Flow-Induced Crystallization Kinetics

As mentioned above, the deformation induced by flow influences the rate of crystallization and thus final morphology of molded products. In order to consider the effect of flow, it is therefore mandatory to model the molecular orientation. A model which resulted to be effective and simple enough to be implemented in simulation software is a nonlinear formulation of the elastic dumbbell model. If $\underset{\sim}{R}$ is the end-to-end vector of a molecular chain and the symbol < > is the average over the configuration space, a fractional "deformation" of the population of dumbbell sub-chains with respect to the equilibrium conformation can be defined as Eq. 5.13:

$$\underset{\approx}{A} = \frac{3}{\left\langle R_0^2 \right\rangle}\left[\left\langle \underset{\sim}{R}\,\underset{\sim}{R} \right\rangle - \left\langle \underset{\sim}{R}\,\underset{\sim}{R} \right\rangle_0\right]. \tag{5.13}$$

The evolution of the conformation tensor $\underset{\approx}{A}$ describing the sub-chain population was obtained by a Maxwell-type equation [54] with a single dominant relaxation time (Eq. 5.14):

$$\frac{D}{Dt}\underset{\approx}{A} - \left(\nabla \underset{\sim}{v}\right)^T \times \underset{\approx}{A} - \underset{\approx}{A} \times \left(\nabla \underset{\sim}{v}\right) = -\frac{1}{\lambda}\underset{\approx}{A} + \left(\nabla \underset{\sim}{v}\right)^T + \left(\nabla \underset{\sim}{v}\right). \tag{5.14}$$

The relaxation time, λ, is allowed to vary with shear rate and temperature (Eq. 5.15):

$$\lambda(T, P, \chi, \Delta) = \frac{\lambda_0 \cdot \alpha(T, P, \chi)}{1 + (a\Delta)^b}. \tag{5.15}$$

A shift factor, α, due to temperature, pressure and crystallinity, χ, is also considered; it is expressed by the modified WLF relationship (Eq. 5.16):

$$\alpha(T, P, \chi) = 10^{\frac{-c_1(T - T_0 - C_3 P)}{C_2 + T - T_0}} \cdot \delta(\chi). \tag{5.16}$$

The difference, Δ, between the two main eigenvalues of the tensor $\underset{\approx}{A}$ is taken as an appropriate measure of the molecular stretch [57].

In the spherulitic regime, the growth rate could be always described by Eq. 5.7, in which only the melting temperature changed by effect of flow. By considering that under steady shear the shear rate can be directly associated to the molecular stretch Δ, in Fig. 5.11 the melting temperatures are reported as function of the molecular stretch parameter.

Once the melting temperature is calculated, the growth rate can be calculated according to Eq. 5.7. In order to complete the morphology development in the stage *ii*, the nucleation rate needs to be evaluated. For polypropylene, a correlation

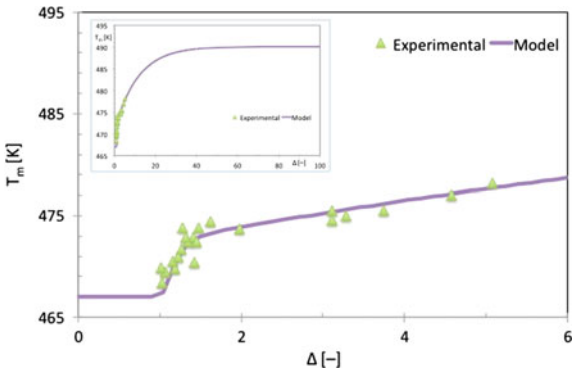

Fig. 5.11 Melting temperature (green triangle symbols) evaluated from steady shear experiments as function of molecular stretch, Δ. Data reproduced from [57]

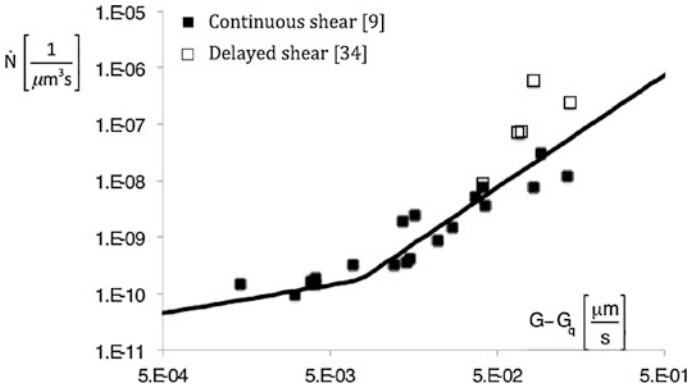

Fig. 5.12 Experimental values of nucleation rate versus excess growth rate under several shear rate conditions (reported as symbols). Data reproduced from [57]

between the excess of growth rate (with respect to quiescent conditions) and the nucleation rate under the same conditions (of shear rate and temperature) was identified in the literature [36, 57]. The existence of such a correlation between growth rate and nucleation rate is consistent with the fact that also nucleation rate is usually described by Hoffman and Lauritzen equation [58, 59]. The correlation adopted between the nucleation rate and the excess growth rate (namely the difference between the growth rate measured under flow and in quiescent conditions at the same temperature) is reported in Fig. 5.12. By adopting the excess growth rate as independent variable, both vertical and horizontal axes are zero in quiescent conditions.

On the basis of this correlation, the nucleation rate can be calculated once the growth rate is known both in quiescent and in flow conditions.

5.4 Injection Molding

5.4.1 Morphology of Injection Molded PP

The morphology distribution inside an injection molded semicrystalline part is made by several layers moving from the surface toward the midplane: a skin layer, where (due to the high cooling rates) the material is quenched and a poorly structured material is found; a shear layer, where due to the strong flow fields highly oriented fibrillar structures are found; a core layer, where spherulitical structures are found, whose dimensions normally increase on increasing the distance from the surface [54, 60–62]. An example of this morphological organization, referred as skin-core morphology [57] is reported in Fig. 5.13. In particular, a thin skin layer composed by globular elements can be found at the sample surface (Fig. 5.13a). A fibrillar layer (sometimes referred to as shear layer) characterized by highly oriented fibrillar structures was found close to the sample surface (Fig. 5.13b). The presence of a transitional region with a gradual change from fibrillar to spherulitical is observed. The presence of spherulitic structures with different dimension in the core region is shown in Fig. 5.13c–e When the morphology is observed by Polarized Optical Microscopy (POM), a dark band at the midplane can be present. This feature is reported in many literature papers referring to the injection molding of polypropylene [54, 63–67], whereas in some other papers, also reporting full width images of the samples, the phenomenon was not present [60, 68].

In a recent paper [57] it was found that in the dark band smaller spherulites are present with respect to the adjacent layers.

The composition of the morphology is responsible for the end-use properties of a plastic part. A local measure of elastic modulus conducted by Indentation and HarmoniX AFM tests [69] revealed that higher values of the modulus are found in the shear layer, intermediate values in the core spherulitic layer and minimum values in the skin layer. As a result, parts with a thick oriented shear layer show higher impact strength, a poorer dimensional stability [70], and a larger yield stress [71]. In contrast, samples with a larger core layer tend to be brittle (Fig. 5.14).

The thickness of each of the layers depends on the processing conditions. In order to elucidate this point, we refer to some injection molding tests reported in the literature [73]. In particular, the tests were carried out with the iPP T30G supplied by Basell. All the details on geometry and experimental procedures are available in the literature [2, 54, 74].

The test conditions are reported in Table 5.2, and each of them differs from the condition named “standard” for the value of just one of the main processing parameters: flow rate during filling, mold temperature and holding pressure.

The effect of molding conditions on the multilayer morphology of injection molded part is evidenced in Fig. 5.15, where pictures of the samples taken in crossed polarized light are shown. The pictures refer to slices taken in a central position in cavity namely P3, and report just one half of the sample width, with the sample surface at the top, and the midplane at the bottom of the images. The

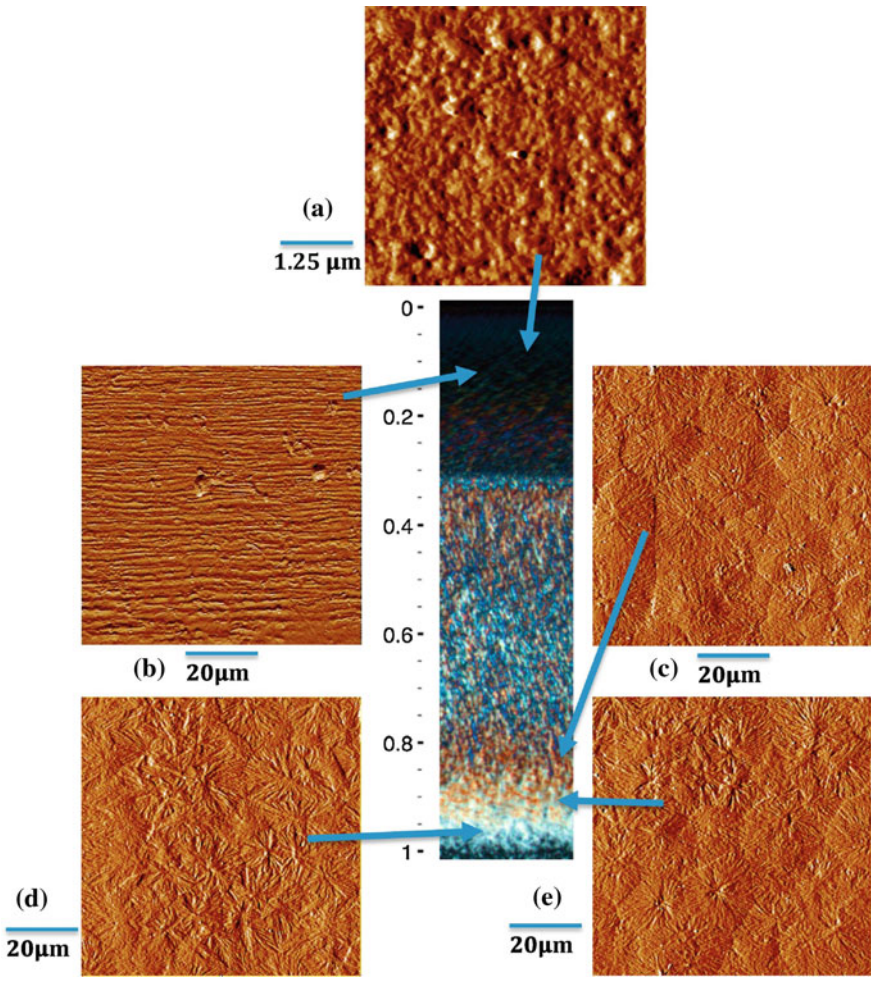

Fig. 5.13 The optical micrograph and AFM amplitude error images of sample "standard" in position P3 (central in cavity). AFM images show details of the morphology along the half–thickness: **a** in skin layer, **b** in the shear layer and **c**–**e** in the core region. Different scan size was adopted for the AFM images. Reproduced from [57]

thicknesses of the shear layers and of the skin layer in position P3 of those moldings are reported in Table 5.3.

In all cases, the flow is parallel to the plane of the slices. In order to clearly identify the position of the layers, beside each optical micrograph a bar reporting the thickness of the skin layer (black in the bar), the shear layer (grey in the bar) and the spherulitic layer (white in the bar) is shown. The skin layer is clearly evident in all cases except for the High T condition. It is worth mentioning that, according to a detailed characterization of the samples [54], when present, the skin layer is

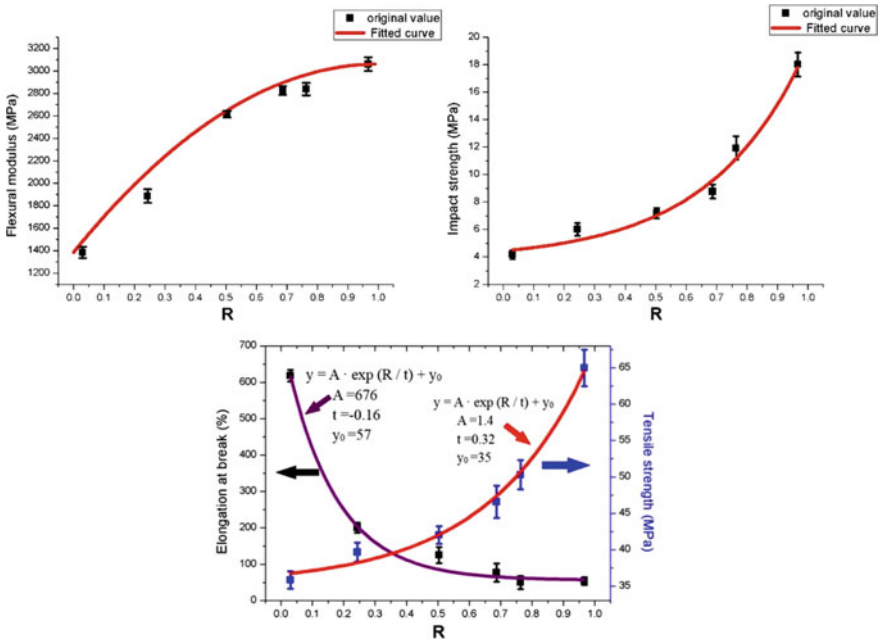

Fig. 5.14 Mechanical properties of different samples of polypropylene versus R (thickness ratio of shear layer to whole sample). Reproduced from [72]

Table 5.2 Processing conditions

	Standard	Slow	High T	High P
Flow rate [cm^3/s]	15	5	15	15
Mold temperature [°C]	30	30	70	30
Holding pressure [bar]	400	400	400	700

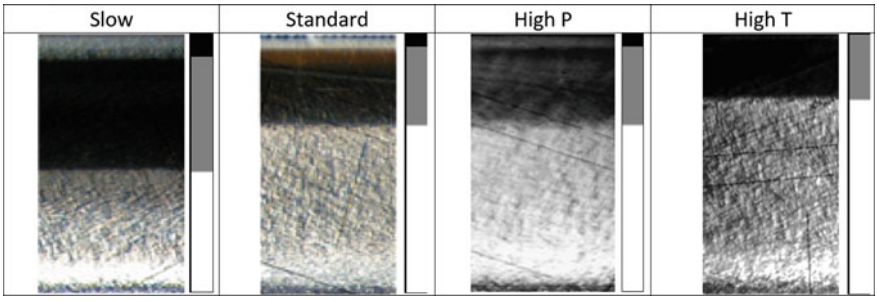

Fig. 5.15 Optical images, in cross polarized light, of the half thickness of the sample in position P3 for all the conditions reported in Table 5.2. The sample surface at the top, and the midplane at the bottom of the images. The thicknesses of the shear layers and of the skin layer in position P3 of those moldings are reported in Table 5.3 [73]

Table 5.3 Thickness of skin and of shear layer for all the conditions considered as measured from optical images reported in Fig. 5.15

	Standard	Slow	High T	High P
Skin layer thickness [μm]	50	80	Not detectable	50
Shear layer thickness [μm]	290	430	250	290

significantly crystalline with a predominance of α phase with few percent of mesomorphic phase. The shear layer appears as the darkest part of the pictures; the core layer, that is formed by spherulitic structures with different dimensions, is instead the lightest one. At the midplane, a darker layer is shown in the optical micrograph of all samples considered in this work.

The morphology developed along the sample thickness is due to the balancing between two phenomena: the molecular stretch which takes place mainly during the filling stage and the cooling rate that determines the solidification. Since the structuring is a kinetic process, when the cooling rate through solidification is very high the material does not have time to achieve a complete structuring. This happens close to the sample surface and determines the formation of a poorly structured skin layer. The thickness of the skin layer is expected to decrease as surface cooling rate decreases, as shown in Fig. 5.15, this happens in the sample sequence conditions slow, standard—high P, high T. The surface cooling rate is expected to be the highest for the slow condition because in that case the both convection and viscous generation, being smaller at any temperature, are less effective to delay the cooling rate through solidification.

5.4.2 Morphology of Micro-Injection-Molded PP

In recent years, plastic molding techniques such as injection molding, which is a suitable process for medium and large-scale fabrication, have been adapted for the necessities of microcomponents fabrication [75], when downscaling systems, products, and their components, the limits of conventional manufacturing techniques are reached. This initiated the improvement of conventional techniques and the further development of new ones, as in the case of the micro-injection molding process. Lateral dimensions in the micrometer range, structural details in the sub-micrometer dimensional level and high aspect ratio (aspect ratio = depth/width) of 10 and above are achieved.

On reducing the thickness of the injection molded parts (having a typical dimension of 1–3 mm) to thin-wall injection molding (typical thickness 300–500 μm), the morphology along thickness tends to maintain the same configuration [76]. The shear layer increases its relative dimension due to the increase of the shear stresses and cooling rates [66]. Moving toward micro-injection molding, with characteristic dimensions of the order of 100 μm, the shear layer extends towards the center of the molding, sometimes resulting in a so called "core-free" part [65], namely the complete absence of spherulitic morphology.

Due to the miniature characteristics of the molded parts, however, a special molding machine and/or auxiliary equipment are required to perform tasks such as shot volume control, process parameters control, injection, packaging of molded parts.

In particular, the rapid control of cavity surface temperature is essential for obtaining a micro-thickness iPP part with an acceptable cycle time [77]. As expected also the resulting morphology, and thus the final properties, could be controlled by the local surface temperature of the mold, as shown in Fig. 5.16.

Furthermore the temperature control of the cavity surface is essential for the replication of micro and nano-features on iPP parts by injection molding [78].

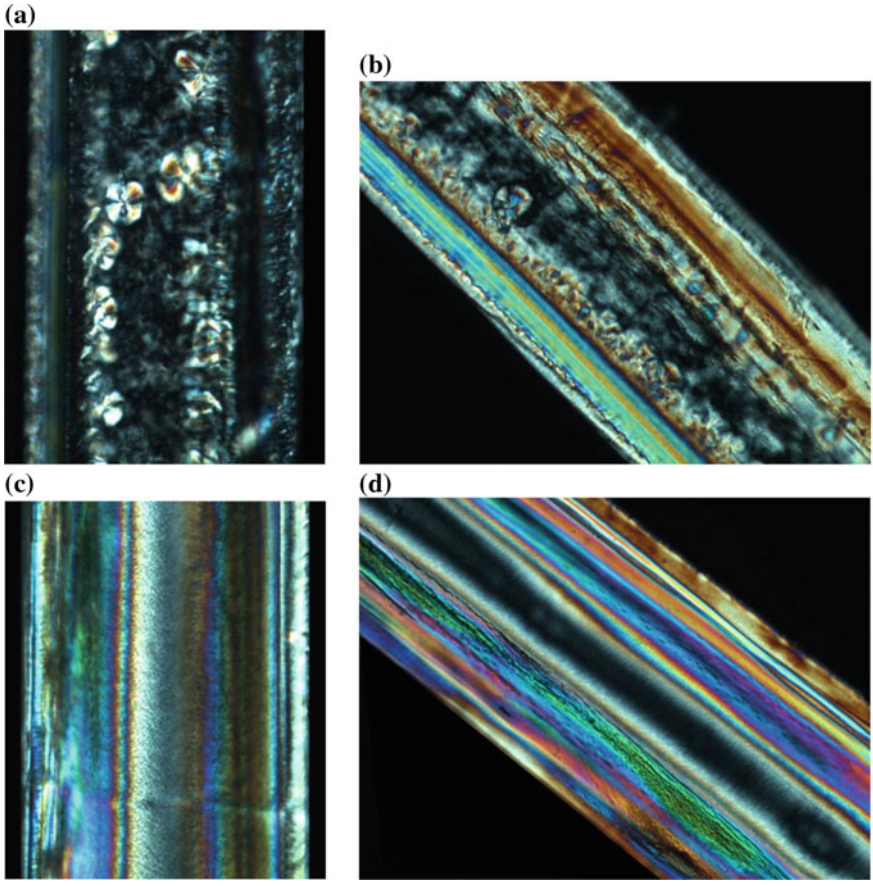

Fig. 5.16 Microtomed slices of molded samples in polarized light. The thickness of the samples is 200 μm. The holding pressure is 200 bar. **a** mold surface 120 °C. **b** same sample as in **a**, after a 45° rotation; **c** mold surface 25 °C, **d** same sample as in **c**, after a 45° rotation. Data reproduced from [77]

5.4.3 Advanced Methods to Control Morphology of Injection Molded Parts

Fast Cavity Surface Heating Technique

The morphology developed in the molded parts is strongly influenced by processing parameters. Molecular stretch distribution at solidification depends on the injection conditions and, therefore, also mold surface temperature. This latter is a key parameter in controlling molecular stretching: if temperature is kept high starting from the filling for a few seconds, the relaxation of the molecular stretching can be calibrated before cooling [79, 80]. At present, the fastest evolution of mold temperature can be obtained by heating devices located just below the cavity surface [77]. Liparoti et al. [69] reported the effect of induced asymmetrical fast surface temperature evolution on the morphology of injection molded isotactic polypropylene (iPP) samples.

An example of cross-section morphology obtained by the optical micrograph of the sample prepared by conventional injection molding (CIM), namely without temperature control (i.e. T_off), is shown at the top of Fig. 5.17. The other morphologies reported in Fig. 5.17 refer to the samples obtained keeping one of the the cavity surfaces (the left one, in the Fig. 5.17) at the temperature of 120 °C for 0.5, 8 and 18 s. The different layers developed along the sample thickness are strongly influenced by the temperature of the cavity surface. In particular, the shear layer moves toward the sample surface and its thickness decreases by increasing the heating time. The skin layer disappears for longer heating times, while with a heating time of 0.5 s the presence of the skin layer is not clearly evidenced from the polarized optical micrograph. Figure 5.17 shows that a heating time of the order of the filling time (0.5 s) is sufficient to lose the symmetric morphology of the sample.

The morphology of the samples has a direct effect on the distribution of mechanical properties along the sample thickness (Fig. 5.18).

The maximum value of the modulus is located in the shear layers. The skin layer shows the lowest moduli and the spherulitic core has intermediate modulus values.

Shear Controlled Orientation Techniques

The first technologies developed to modify the morphology of the molded parts, were based on the application of a suitable shear or elongational flow field to the solidifying melt that facilitates and enhances molecular alignment. To fabricate polymer products with high performance the shear controlled orientation injection molding (SCORIM) techniques was developed by Allan and Bevis [81, 82]. Successive shear could increase the degree of orientation of melt as much as possible, thus allowing a high possibility of forming shish kebabs in the moldings. The SCORIM equipment consists of a device that is attached to the injection nozzle and is composed of a hot runner circuit that divides the melt stream into two channels where two hydraulically actuated pistons are operated during the holding pressure stage. The SCORIM double live-feed is shown in Fig. 5.19. Compared to CIM, where the molten material solidifies under the influence of an almost static pressure, in SCORIM, the polymer melt is continuously displaced inside the mold

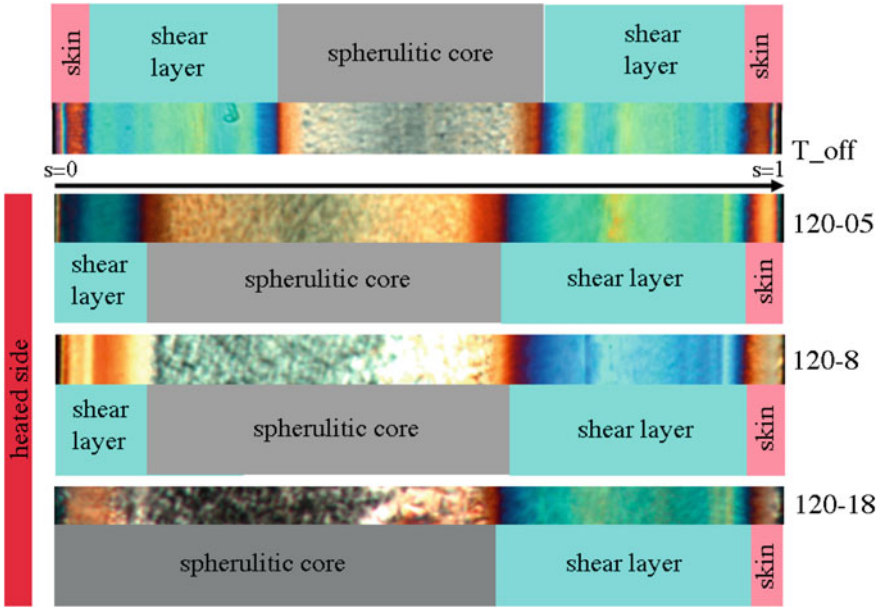

Fig. 5.17 Optical micrographs of the samples from test runs T_off, 120-05, 120-8 and 120-18. The heated side is reported on the left most of the figure. Data reproduced from [69]

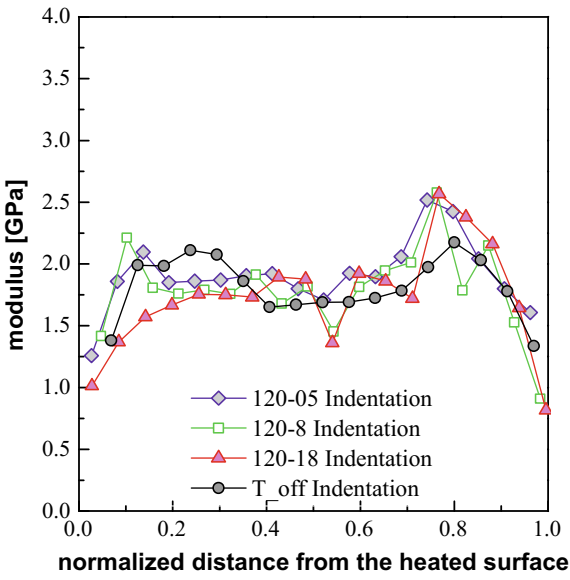

Fig. 5.18 Elastic modulus distributions (obtained from indentation analyses) along the sample thickness for the samples T_off, 120-05, 120-8 and 120-18. Data reproduced from [69]

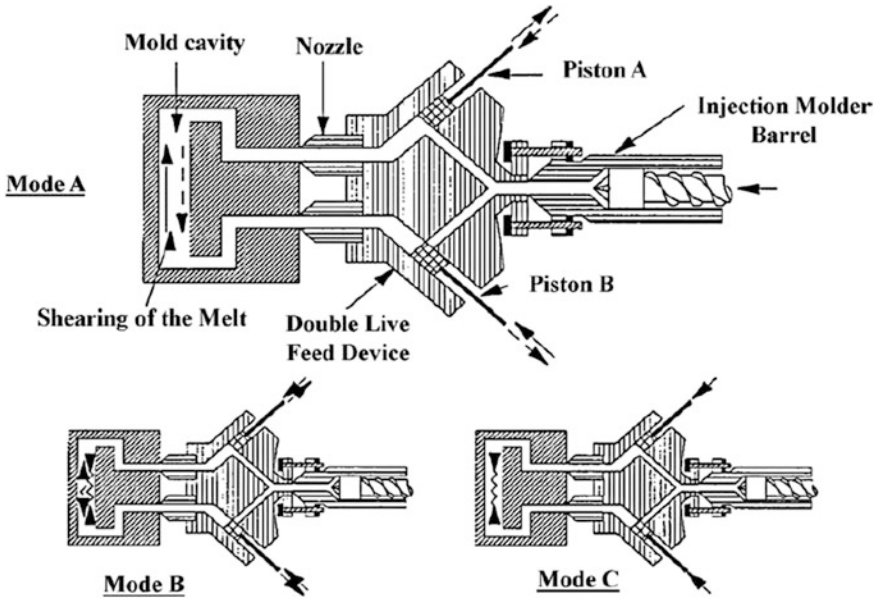

Fig. 5.19 Scheme of the function of the SCORIM procedure along with the three basic modes of operations (A, B and C)—Mode A: the pistons are activated 180° out of phase; Mode B: the pistons are activated in phase; Mode C: the pistons are held down at a constant pressure. Data reproduced from [81]

cavity by the action of the hydraulic pistons. This causes, as the solidification takes place progressively from the skin to core regions, a continuous shear imposed to the melt. This effect is accomplished using the SCORIM Mode A of operation that corresponds to the out-of-phase oscillation of the pistons. Other possible modes include Mode B (in phase oscillation of the pistons) and Mode C (compression of the pistons at a constant pressure). These operational modes can be combined sequentially in several stages during processing to lead to a different shear field at melt/solid interface.

The γ-phase was found to form in highly oriented SCORIM iPP samples [83], with a marked enhancement of the preferred orientation of the α-phase and percentage crystallinity when compared with CIM iPP. Compared with CIM, SCORIM technique results in more pronounced molecular orientation, leading to the substantial increase in Young's modulus of SCORIM moldings [84]. By controlling the processing parameters, it is possible to enhance the stiffness without loss of tensile strength for SCORIM moldings: the moldings prepared by SCORIM exhibit an increase in impact strength of up to four times, as well as gaining remarkable increase in Young's modulus.

A comparison of failure surfaces of CIM and SCORIM moldings are shown in Fig. 5.20 [71]. It can be seen that almost all CIM moldings exhibit four distinct layers: the skin, the oriented zone, the layered core region, and the central core

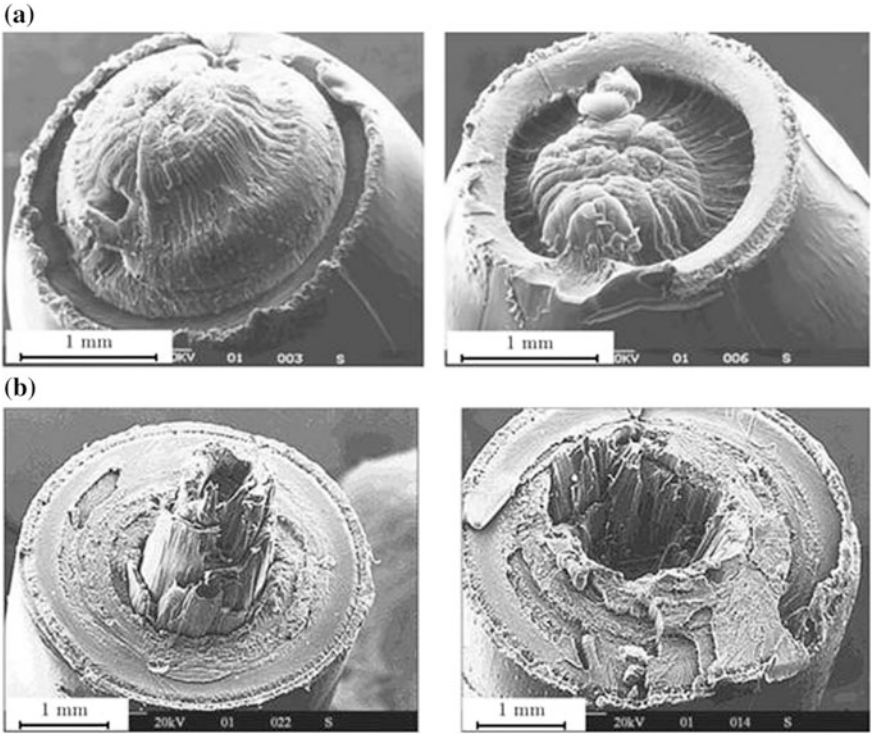

Fig. 5.20 Two opposite tensile failure surfaces of: **a** CIM moldings; **b** the majority of SCORIM moldings. Data reproduced from [71]

region. While the major SCORIM moldings exhibit five distinctive layers: the skin; the sub-skin; the oriented zone; the transition zone between the oriented zone and the core; and the core region. The core region is ductile, so there is a pit in the center of a tensile failure surface.

The results of microstructure investigation indicate that there exists γ-phase of SCORIM iPP moldings with pronounced molecular orientation. So, the common view that iPP has only α- and β-phases in commercially produced moldings is challenged. The presence of γ-phase in injection moldings is indicative of enhanced Young's modulus and tensile strength, and it is consistent with the results of mechanical characterization. Another reason for the substantial increase in Young's modulus of moldings produced by SCORIM is the more pronounced molecular orientation compared to CIM samples. The calculated results from DSC and WAXD show that SCORIM moldings contain less β-phase and exhibit greater overall crystallinity than CIM moldings. The difference in the relative proportions of α-, β-, and γ-phases is marked and depends on processing conditions and the molding method.

The OPIM technique (oscillating packing injection molding), also called dynamic packing injection molding (DPIM) or oscillatory shear injection molding

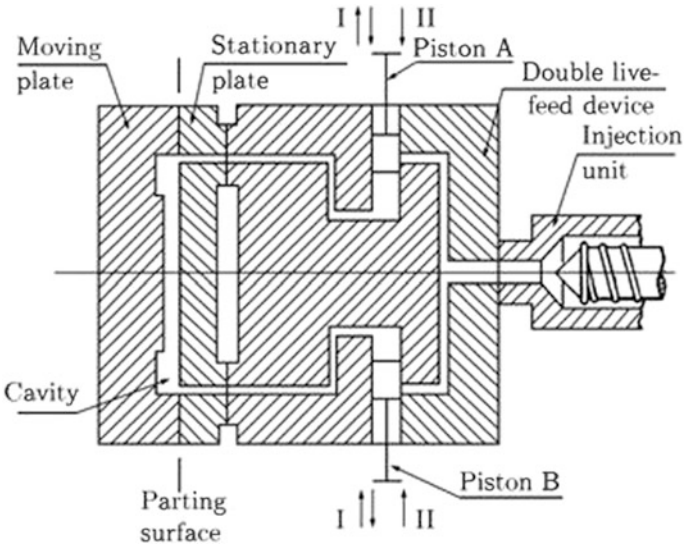

Fig. 5.21 Device for DPIM (I: two pistons reciprocate with a difference of 180 °) and SPIM (II: two pistons push forward simultaneously) moldings. Data reproduced from [85]

(OSIM) in some articles, was developed by Shen's group based on SCORIM [85]. The scheme of the OPIM device is shown in Fig. 5.21. Similarly, to the SCORIM technique, there are three movement modes for the two hydraulically actuated pistons to generate a corresponding shear stress field during the cooling solidification of melt in cavity, thus different morphologies in moldings. Contrasting to SCORIM where the multi-piston oscillating packing unit was an independent device, OPIM adopted hot runner system, and combined double live-feed device to injection molding machine, which greatly improved and streamlined the SCORIM device.

The mechanical properties of iPP can be greatly enhanced using OPIM under low pressure [86]. Samples prepared by OPIM under elongational test exhibit a brittle tensile failure, whereas the samples prepared by CIM are ductile. The increase in mechanical properties is mainly attributed to perfect spherulites, the shear-induced shish kebab structure (also confirmed by the high temperature peak of double peaks in DSC curves), and the enhanced orientation of molecular chains. The holding mode has strong influence on the mechanical performance of self-reinforced iPP, while the other processing variables such as oscillating frequency, oscillating pressure, melt temperature and holding time, have little influence on the mechanical properties of OPIM iPP moldings.

The OPIM moldings are anisotropic [87], the stress-strain curves show typical brittle failure in the TD and relative ductile failure in MD as also confirmed in Fig. 5.22 were the SEM micrographs of tensile fracture surfaces are reported.

In Fig. 5.22a the tensile fracture surface of the outer shear region in MD is shown, and it exhibits a very rough and uneven failure surface with voids and

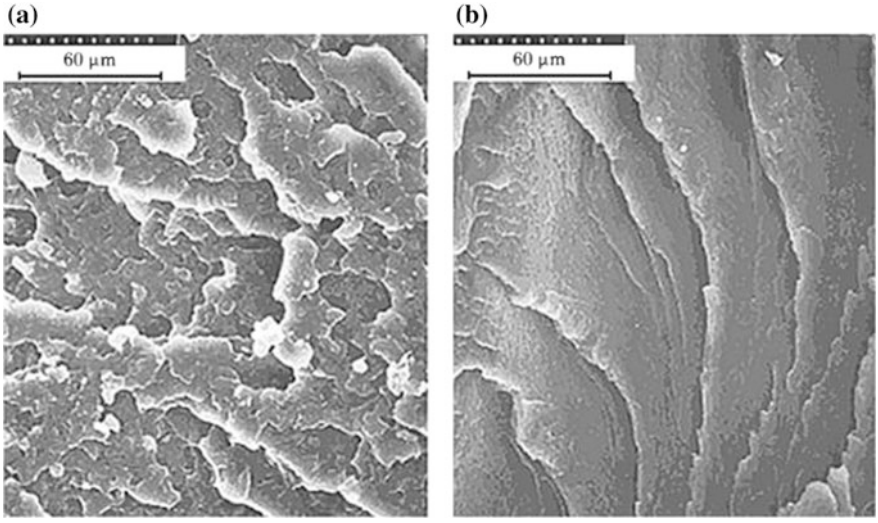

Fig. 5.22 SEM micrographs of the tensile fracture surface of OPIM moldings in **a** MD, and **b** TD. Data reproduced from [87]

crazes. In Fig. 5.22b the tensile fracture surface in TD exhibits a relatively planar failure surface but with delamination. The mechanical property is consistent with the microstructure observed. iPP samples processed by OPIM exhibit interlocking shish kebab structure within the outer shear region and a much smaller spherulitic core region with respect the CIM samples. Moreover, the OPIM moldings contain both α and β crystalline phases (also contained in CIM samples) and γ crystallites. The OPIM moldings exhibit the highest α-phase orientation and largest proportion of β-phase content in the outer shear region.

Analysis by 2D-WAXD OSIM show that OSIM samples present, at a given depth, higher degree of molecular orientation and that the α- and γ-crystals appear at different depths of the samples. Moreover, estimation of the overall crystallinity shows that, due to the stronger shear imposed, higher level of crystallinity are reached in the OSIM samples with respect the CIM samples [88].

The fraction of γ-crystal, f_γ, with respect to α-crystal in samples, was calculated and the distribution of f_γ through the depth of samples was shown in Fig. 5.23.

From the distribution curves of f_γ, it can be seen that the spatial distribution of γ-crystal is different for CIM and OSIM samples. The f_γ of CIM samples increased monotonously in outer regions along the direction from skin to core. However, OSIM samples have almost the same minimal f_γ ($\sim$ 0.57) in the skin and core regions, and a maximum in the intermediate regions. The phenomenon of less γ-crystals in the inner regions of OSIM samples contradicts the widely accepted point of view that f_γ should be high when the cooling rate is low caused by shear heating.

OSIM is reported [89, 90] as a successful method for controlling the structure and morphology formation of iPP and tuning its mechanical properties. The competition of shear-induced crystallization and β-nucleant results in the hierarchic

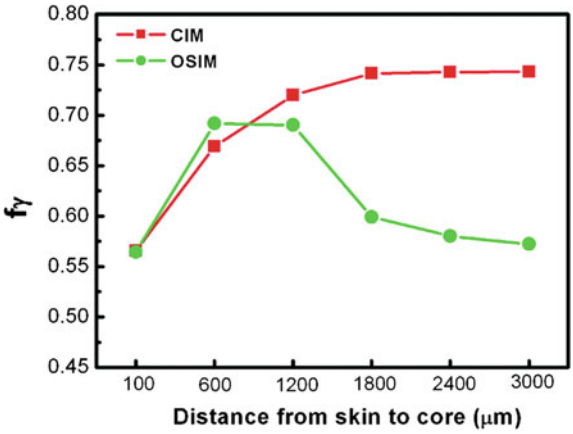

Fig. 5.23 Fraction of γ-crystal with respect to α-crystal, f_γ, evaluated from the X-ray diffraction profiles from skin to core region of CIM and OSIM samples. Data reproduced from [88]

structure of the OSIM β-iPP sample, which is like that of bamboo, which has a tight and fibrillar outer layer, as well as a soft and loose inner layer. In the outer layers (skin and intermediate layers) highly oriented α-form crystals (shish kebabs) are present, while in the core layer high-proportion β-form spherulites are present. In the skin layer, the orientation should be ascribed to the shear imposed on the melt before the gate of mold freezes. In the core layer, as the gate of the mold freezes, iPP is still in melt state, so that the molecular chains have enough time to relax. In this case, the β-nucleating agent takes effect, leading to the formation of β-crystals.

Vibration-assisted Injection Molding

It is quite well known that the external force field can affect the rheological properties of polymer melt. By introducing a vibration field to the polymer melt, it is not only able to depress the shrinkage of molded products in injection molding and improve the surface quality of extrudates [91, 92], but also to substantially increase the orientation potential of polymers by reducing the amount of relaxation [93], therefore achieving control of microstructure and morphology, and enhancement of mechanical performances of the final products. The most important parameters in vibration-assisted injection molding/extrusion are vibration frequency and amplitude. According to the vibration frequency, vibration field can be divided into mechanical vibration and ultrasonic vibration. The frequency of ultrasonic vibration is in the range of 20 kHz and more, while the frequency of mechanical vibration is much lower than that of ultrasonic vibration, which is always within 0–100 Hz. Also, mechanical vibration can be divided into pressure vibration and shear vibration. In the pressure vibration processes, polymer melt is periodically compressed and released, while in the shear vibration processes, a periodical oscillating shear field is imposed on polymer melt.

Li et al. studied the effects of vibration injection molding (VIM) on the morphological structure and mechanical properties of PP [94, 95] by superimposing a pulse pressure on polymer melt during the injection and holding pressure stages. The device and working principle are depicted in Fig. 5.24.

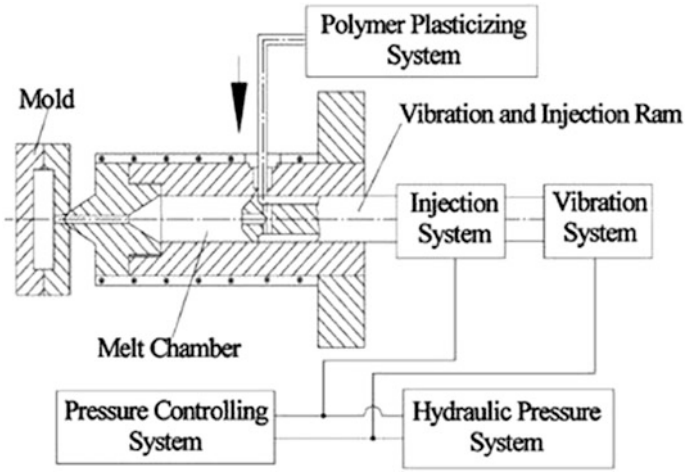

Fig. 5.24 Schematic diagram of the pressure vibration injection molding (VIM). Data reproduced from [95]

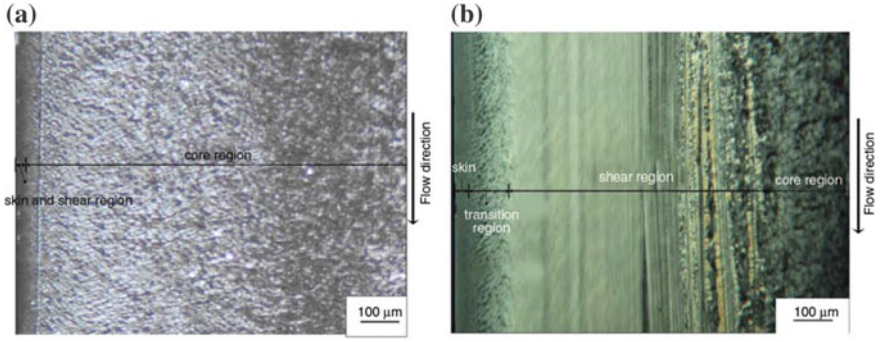

Fig. 5.25 Effect of vibration on the morphology of an injection molded PP sample. **a** CIM, **b** Vibration injection molding. Reproduced from [96]

The ram itself is a part of both the injection and vibration systems. The main processing parameters are vibration frequency and vibration pressure amplitude, which is in the range of 0–2.5 Hz and 0–75 MPa, respectively.

The samples prepared via VIM showed that with the increase of vibration frequency, the yield strength, Young's modulus and impact strength steeply rose firstly, afterwards, remained at a plateau, while the elongation at break decreased firstly and then ramped up. The yield strength and impact strength increased monotonously while the elongation at break decreased remarkably with increasing vibration pressure amplitude. As for morphology, the random distribution of spherulites, obtained by CIM, was changed into parallel lamella perpendicular to the melt flow direction for the VIM-produced samples (Fig. 5.25).

It is believed that the effect of melt vibration on the morphology was to orientate the structure unit along the melt flow direction, especially under the processing conditions with high vibration pressure amplitude. The results also showed that, for VIM, accompanied with higher crystallinity, the melting peaks shifted to higher temperature, meaning more perfect crystalline existed.

5.5 Modeling Morphology in Injection Molded Parts

In the injection molding, polymers are processed under severe conditions (high cooling rates and pressures, strong and complex flow field) and this complex thermomechanical history experienced by the polymer induces a local order of macromolecules. For semi-crystalline materials, highly oriented lamellar crystallite microstructures are detected near to the molding surface, namely in the shear layer where the shear stress levels are high, whereas isotropic spherulitic structures are detected far from the wall, i.e. in the core layer where the shear stress decreasing to very small values. The level of the order reached locally by the macromolecules and thus the structure formation is the result of the competition between the shear deformation, i.e. the flow characteristic time, and the cooling rate, which determines thermomechanical and crystallinity histories and thus the relaxation time.

5.5.1 Fibrillar Morphology

Depending to the processing conditions adopted, sometimes an additional layer, namely a skin layer, is found on the molding surface, before the shear layer, characterized by less oriented crystalline structure. In this layer due to the very high cooling rates, the macromolecules are quenched does not have enough time to organize themselves in highly oriented structures as in the deeper shear layer. It is noteworthy that along the molding thickness some transitional layers are recognized between the skin-shear-core layer structure previously depicted. Experimental investigations have confirmed that in presence of flow under certain threshold the morphology evolution maintains its quiescent characteristic and above a second threshold morphology evolution is modified and oriented structures (shish kebabs) are formed in the crystallizing polymer.

One of the first attempts to model the development of crystallinity and morphology in the injection moldings of iPP was conducted by Isayev et al. [97, 98]. They proposed a unified crystallization model in which the effect of flow on the crystallization kinetics is accounted for. The model, that adopts the "competing mechanisms" of crystallization in terms of the induction time indices, was able to distinguish between the highly oriented skin layer and spherulitic core in the moldings. In particular, they assumed that the polymer solidified in different morphologies depending upon the competition between the degree of supercooling and the molecular orientation caused by the thermomechanical history.

A few years later, at the beginning of the 2000s, Zuidema et al. [99] implemented a model which considered the process of spherulitical nucleation and crystal growth combined with flow-induced crystallization process described by modified version of the model presented by Eder et al. [56, 100]. The Eder's model was adopted for flow-induced crystallization being able to describe the formation of thread-like nuclei (shish) on which lamellae grow mainly perpendicularly (kebabs). In particular, the modification proposed consider the second invariant of the elastic tensor as the driving force for flow-induced nucleation and crystallization instead of the shear rate. To consider flow-induced orientation and stretch of molecules the viscoelastic behavior of polymer is described with a Leonov model [101, 102].

Kennedy and Zheng [103] also modeled the effect of flow on crystallization kinetics and on morphological changes. They considered an effect of flow on nucleation rate related to the excess of free energy and an Avrami index as a function of the second invariant of the second order orientation tensor depending. With the adopted relationship, the Avrami index equals to 3 at a random orientation state, corresponding to spherical growth; and equals to 1 at the perfectly aligned orientation state, corresponding to rod-like growth. For the semicrystalline phase the orientation evolution is described with the rigid dumbbell model.

In the past decade, it was demonstrated that the formation of shish kebabs can be observed at high flow rates. In particular, the chains with a longer relaxation time in the polymer ensemble have to be stretched by flow and thus the shear rates exerted on the chains have to be higher than a critical value that is the inverse of the Rouse time. On the other hands, clear criteria to be adopted to describe the transition from spherulites to the oriented morphologies of shish kebabs was not found. Recent developments [40, 104] have demonstrated that the parameter responsible for the onset of the oriented morphology is the mechanical work; if a polymer has experienced more than a threshold value of the mechanical work oriented shish kebab morphology can be formed. It is important to notice that the threshold work performed at shear rate not above the critical value it is not sufficient to form oriented shish kebab structure. Thus, both the two conditions have to be respected to form oriented shish kebab structure: the threshold work has to be performed above the critical value of the shear rate.

More recently for the injection molding a modification of the above work criterion was developed [73]. The model for fibrillar crystallization mentioned above is adopted with the following additional simultaneity criterion: the whole amount of work has to be done while the molecular stretch is above a critical value; furthermore, if the molecular stretch is let to relax below that critical value, all previous work has to be cancelled in the accounting for the critical work. The criterion that the work performed before the stretch reaches its critical value is not relevant to the purpose of achieving fibrillar crystallization appears physically grounded. In many processing conditions, the polymer melt is oriented first and then has the time to (partially) relax before being oriented again. If the relaxation were complete, it is obvious that the whole previous history does not have any effect of what happens next. This would mean that the time integral of the work alone is not a suitable criterion for describing the phenomenon in complex flow conditions.

The "simultaneity" criterion is consistent with the results of the experiments conducted in literature and reported in [37, 40, 104] that consider an isothermal constant rotating parallel-plate flow, under steady shear rate conditions, if transient flow is negligible. In all the proposed experiments for the radii of the plate in which the fibrillary morphologies formation is observed, the most of the viscous work was actually performed when the steady critical shear rate (molecular stretch) was already achieved and thus the simultaneity criterion is automatically assured.

Comparisons were conducted between experimental results of shear layer thickness observed in different injection molding conditions and prediction obtained on the basis of criteria founded on a critical (shear rate) stretch value and on a critical work value. From the experimental observation was found that, starting from the sample surface, the presence of a skin layer, a shear layer and a spherulitical core layer. The molding conditions that were adopted strongly influenced the thicknesses and the positions of the different layers. From the integral of the viscous work and the final stretch distributions together, predictions of the shear layer thickness and its position was obtained considering all the points presenting both values higher than the chosen threshold (critical values). It was observed that a reasonable comparison with the thicknesses and the positions of the shear layers observed cannot be obtained whatever realistic choice would be done for the two critical values.

Considering the "simultaneity" criterion, the fibrillar crystalline structures can form when the time integral of the viscous work, calculated when the molecular stretch is constantly larger than its critical value, reaches a work threshold. If the stretch relaxes below the its critical value, the work is set to zero again. By plotting the final distribution along the moldings thickness of the time integral of the viscous work it was found that the work threshold mainly influences the thickness of the skin layer whereas the critical value of the stretch substantially affects the time integral of the work close to the midplane, where the molecular stretch is low. It was shown that the simultaneity criterion is suitable to satisfactory describe both the skin and the shear layer thickness for all the considered molding conditions if appropriate values of critical stretch and work threshold are selected.

5.5.2 Distribution of Spherulite Diameters

The final distribution of the spherulite distribution in the gapwise direction is strongly dependent on the thermal and flow histories experienced by the polymer. At the location where cooling rate are higher, i.e. from the core region toward the skin, the diameter of the spherulites become smaller because spherulite growth has smaller time to proceed, nucleation density becomes large and final spherulite dimensions remain small, because they are limited by impingement. The effect of flow on the final distribution of spherulite diameters depends on the competition of two mechanisms. The final dimensions of the spherulites are controlled by the number of active nuclei which are depending not only on the nucleation rate, but

also on the evolution of crystallinity that depends on the nucleation and growth rate. It is well known that flow induces an enhancement of nucleation and of crystallinity. Thus if the effect of flow on the nucleation rate is prevalent, the spherulites diameter decreases by effect of flow induced crystallization. If the effect of flow on the crystallization is prevalent the spherulites diameter increases by effect of flow induced crystallization. In fact, the growth rate is considered in the evolution of the crystallinity with a power 3. This implies that any nucleus quickly occupies a large portion of the space, thus impeding to other nuclei to fall into amorphous regions and to generate other spherulites. Micrographs of slices were taken by a polarized optical microscope (POM) along the gapwise direction [57]. The skin-core morphology of the samples was evident, with a not oriented skin layer about 50–100 μm thick at the sample surface, an oriented fibrillar layer closer to the sample surface (the so-called shear layer) and a spherulitic core. Furthermore, a dark band at the midplane was found. The same phenomenon was reported in some literature papers referring to the injection molding of polypropylene [63–67] without any comment, whereas in some other papers, also reporting full width images of the samples, the phenomenon was not present [60, 68]. The nature of the dark band is difficult to understand. In the literature, it was reported that the thickness of this band increases on increasing the distance from the gate [54], and tends to disappear on increasing the mold surface temperature [54, 69]. Deeper investigation of this dark band showed an unexpected behavior, i.e. a reduction of the spherulite diameters in the region close to the sample half-thickness.

5.5.3 *Simulation of Morphology Development in Injection Molded IPP: A Case Study*

An accurate prediction of morphology distribution inside injection molded parts of semicrystalline polymers is surely a key issue in polymer processing. Indeed, many of the properties of the solid molded parts depend heavily on the distribution of morphological parameters [12, 105] such as for instance spherulite size distribution [106] or the presence of oriented layer induces anisotropy and other changes in mechanical properties [107]. Therefore, the production of high quality polymeric parts in injection molding, which is a sector in great expansion, requires the capacity of being able to predict not only the thermomechanical histories experienced by polymer during the processing but also these morphological features.

A reliable description of morphological evolution in crystalline materials during injection molding process should, therefore, necessarily account for all major crystallization process and capture the main features of melt morphology evolution under both quiescent and processing conditions (various shear and cooling rates), as well as the complicated interaction between crystallinity and flow.

The major challenging problems on this topic include the following:

- modeling of crystallization phenomena under non-isothermal, quiescent and flow conditions;
- understanding of the mechanisms governing crystallization-induced microstructure development;
- study of physical properties of the polymer before and after the crystallization.

The task is particularly challenging, since during injection molding crystallization, and thus morphology evolution, takes place under severe thermomechanical histories, namely high pressure, fast cooling rates. All these effects must therefore be taken into account in the quiescent model describing the crystallization kinetics. Moreover, the effect of flow on the crystallization process has to be accounted for.

When external flow is applied, for example, during molding processes, molecular chains will orient along preferential directions by the flow. This orientation of macromolecules can cause different properties of crystals in different directions. Therefore, one of the biggest challenges concerns the reliable prediction of molecular orientation during processing.

Furthermore, since polymer properties (above all rheology and density) are function of crystallinity, the thermomechanical history which determines crystallinity is in its turn depending on crystallization. This means that for a correct prediction of final morphology in injection molded parts a suitable model for crystallization kinetics in processing conditions (which is already a quite challenging task) is not enough: it is also necessary to use a software which describes the evolution of the main variables during processing and can keep into account, through specific sub-models, the effect of crystallinity on the relevant material properties [108]. Just for sake of clarity, an incorrect description of crystallization kinetics gives rise not only to a wrong prediction of final morphology, but also to an inaccurate calculation of the pressure evolution inside the cavity, which is normally considered as a primary goal of simulation.

As last remark, it should be clear that predictions for injection molding process are obtained extrapolating all the constitutive equations and model identified to describe the polymer behavior well beyond the experimental ranges, within which each model and equation had been identified.

Numerical simulations of the molding tests described in the Sect. 5.4.1 were conducted adopting the UNISA code that considers the one–dimension laminar flow of a viscous non–Newtonian fluid in non–isothermal conditions. The wall slip phenomena is not taken into account. The process is considered symmetric with respect to the midplane. In the energy balance, the convective term along the flow direction, the conductive term along the sample thickness, the crystallization latent heat and the viscous generation are considered. A surface heat transfer coefficient is assigned. The geometry is schematized as a series of rectangular or cylindrical elements.

The process is simulated into two stages: filling and packing/cooling. During the filling stage the material is considered incompressible and the flow rate is imposed. The fountain flow is not implemented but the variables at the flow front are

averaged on the basis of velocity (i.e. cup-mixing variables are considered at the front). During the packing stage, the material is considered compressible and the flow rate, at each position, is determined by the downstream densification. During the cooling stage the velocity field is annulled and pressure evolution is evaluated on the basis of the pvT behavior of the material accounting of crystallization kinetics. The field equations adopted for the numerical simulation are reported in [109, 110].

Details of the constitutive equation adopted (including the values of the constants) are reported in [111]. All the constitutive equations of that iPP resin (T30G) were recently revised [57] on the basis of data published after the publication of the paper which analyzed those injection molding tests for the first time [2, 54].

The effect of flow on crystallization kinetics is accounted through a stretching parameter, as specified elsewhere [57]; the equations for the evolution of the stretch parameter are summarized in the Sect. 5.2.3. The effects of crystallinity on viscosity and density are taken into account. Consistently, the UNISA code adopts a solidification criterion based on the crystallinity. At last, effect of pressure on viscosity, density and crystallinity are considered. The effect of mold deformation can be accounted for [110].

Predictions obtained with the software UNISA has been compared with experimental pressure data acquired during the injection molding process and with experimental morphological distribution (in terms of final crystallinity and spherulite diameters distribution along the gapwise direction and thicknesses and positions of the shear layer).

Predicted pressure evolutions are compared in Fig. 5.26 with the experimental evolutions collected in the five positions along the flow path during the process. In particular diagrams reported on the top (a and b) refer to the condition “standard”, those at the bottom (c and d) refer the condition “slow” as reported in Table 5.2. Comparison of the rightmost diagrams with the leftmost ones allows to identify the relevance of FIC in the predictions of the thermomechanical histories. Although the predictions obtained with and without FIC seem quite similar, at a closer look some significant differences are detected. For both the conditions, the predictions carried out considering the quiescent crystallization present an overestimation of the gate sealing time which is evidenced by a slower decreasing trend of all the predicted pressure curves in the cavity at times longer than about 10 s. A better description of gate sealing time and of the pressure evolutions is instead achieved considering the FIC in the process simulation. The improvement is significant, even if an underestimation of the pressure drop across the gate remains the main difference between data and simulations.

Comparison of predicted and measured final crystallinity distributions close the sample wall are reported in Fig. 5.27. In particular, considering the “standard” test, in Fig. 5.27 are reported distribution of measured α and mesophase and overall crystallinity compared with the predicted distributions obtained considering a quiescent crystallization model (on the left) and the effect of the FIC (on the right).

The measured IR overall crystallinity distribution shows lower value in a layer close to the sample wall (up to 30 μm from the sample wall) where the polymer

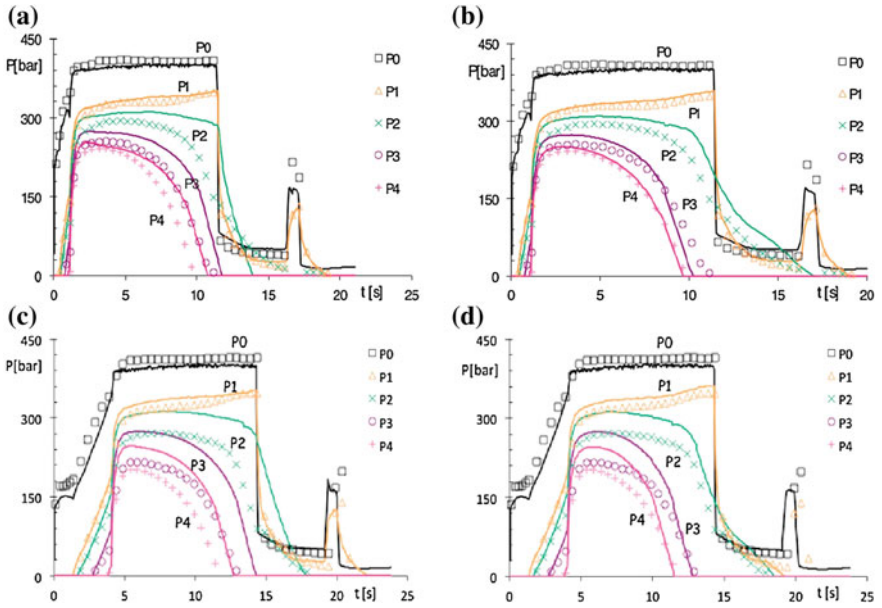

Fig. 5.26 Comparison of pressure evolutions, acquired in the five positions along the flow path during the process, both in "standard" and "slow" condition, with the predicted ones. In particular, for the "standard" condition, predictions are obtained neglecting (**a**) and considering the FIC (**b**); for the "slow" condition, predictions are obtained neglecting (**c**) and considering the FIC (**d**). Data reproduced from [57]

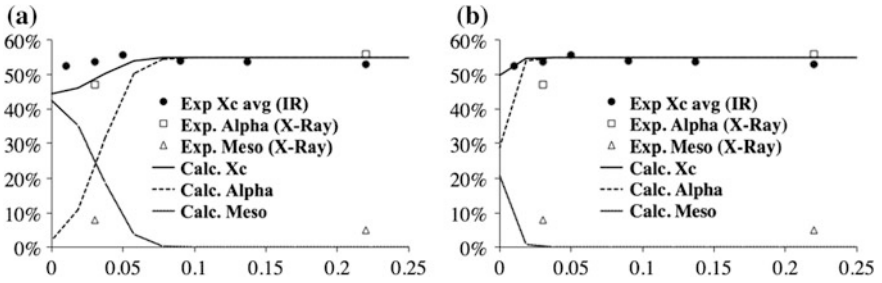

Fig. 5.27 Comparison of the measured final distributions of overall crystallinity, α and mesomorphic phase along the distance d, measured in mm, for the "standard" condition, with the predicted ones. In particular, predictions are obtained neglecting (**a**) and considering the FIC (**b**). Data reproduced from [57]

experienced a very high cooling rate; in the remaining thickness of the sample the crystallinity is constant and equal to the equilibrium value of α phase (namely 55%). The mesophase content is about 10% only close to the sample wall whereas α phase content is prevalent as the distance from the sample wall increase. The effect on the predictions obtained considering the FIC is evident. The thickness of

the quenched zone close to the sample wall is sensible reduced (about halved) with respects to the simulations conducted neglecting the FIC. Therefore, the predicted overall crystallinity distribution tightly describes the experimental data. Furthermore, the α phase distribution predicted has recovered the intense effect of the cooling rate close to the sample wall and now correctly a prevalence of the α phase content is predicted along the whole sample thickness as shown by the performed X-ray analysis.

Comparison of final distribution of crystallinity with predictions obtained considering FIC for all the other tests considered are reported in Fig. 5.28. Predictions of the overall crystallinity in the core and the two phases content correctly describe the measured data. The effect of the processing conditions on the quenching zone thickness is very well predicted. In the "High T" test due to the high mold temperature the cooling rate does not have quenching effect on the material that completely crystallizes to its equilibrium value also near to the sample wall. In the "slow" test due to a lower flow rate the FIC effect on the α crystallization kinetic is not adequate to compensate the effect of the high cooling and therefore the thickness of the quenching zone increase. Only in a thinner zone of about 10 μm the mesomorphic phase content prevails on the α phase content. In the "High P" test, the higher packing pressure effect (that tends to reduce the α phase kinetic at the crystallization temperature in the zone close to sample wall) is coupled with the cooling rate effect; together they counteract the FIC effect more efficiently close to the sample wall with respect the "standard" test and an increase of the quenching zone thickness is predicted.

A comparison between experimental and predicted spherulite diameters is shown in Fig. 5.29 for "standard" and "slow" sample. The predicted spherulite diameters were obtained neglecting and considering FIC. Close to the sample wall the presence of the shear zone, characterized by the presence of fibrillary structures, was observed; in this region, no spherulites are detected. The thickness of this region, measured by the analysis of the images reported in Table 5.3, is marked by a vertical line in the diagrams of Fig. 5.29.

For Fig. 5.29, the left diagrams refer to the predictions carried out by considering the quiescent crystallization kinetics. It can be noticed (Fig. 5.29a, c) that, also neglecting the FIC, the measured distribution of spherulitic dimensions is satisfactorily described by the predictions. The diameters increase as the distance from the sample wall increase due to the decrease of the cooling rate. However, the decrease of the dimensions at the midplane is not captured by quiescent simulations.

If FIC is considered (Figs. 5.29b, d), some significant improvements are observed.

First, in the core spherulitic region, far from the sample midplane, spherulites predicted considering FIC have larger diameters with respect to those predicted by using the quiescent kinetics. Due to FIC the crystallization takes place at higher temperature with respect to the quiescent predictions and both the nucleation rate and the growth rate are enhanced by flow. With the specific correlation between growth rate and nucleation rate adopted, the spherulites generated, due to the flow enhanced growth rate, quickly occupy all the space available for the crystalline α

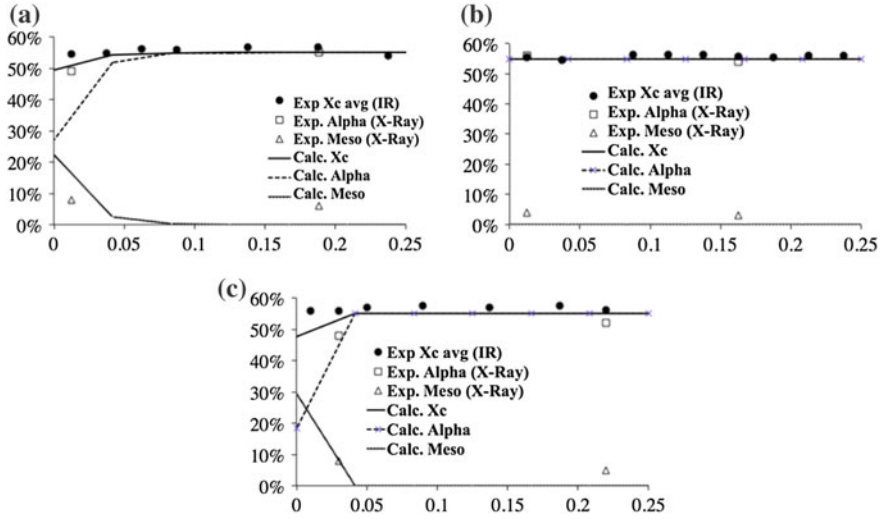

Fig. 5.28 Comparison of the measured final distributions of overall crystallinity, α and mesomorphic phase along the distance d, measured in mm, and the predicted ones (obtained considering FIC) for the "High P" condition (**a**), for the "High T" condition (**b**) and "slow" condition (**c**). Data reproduced from [57]

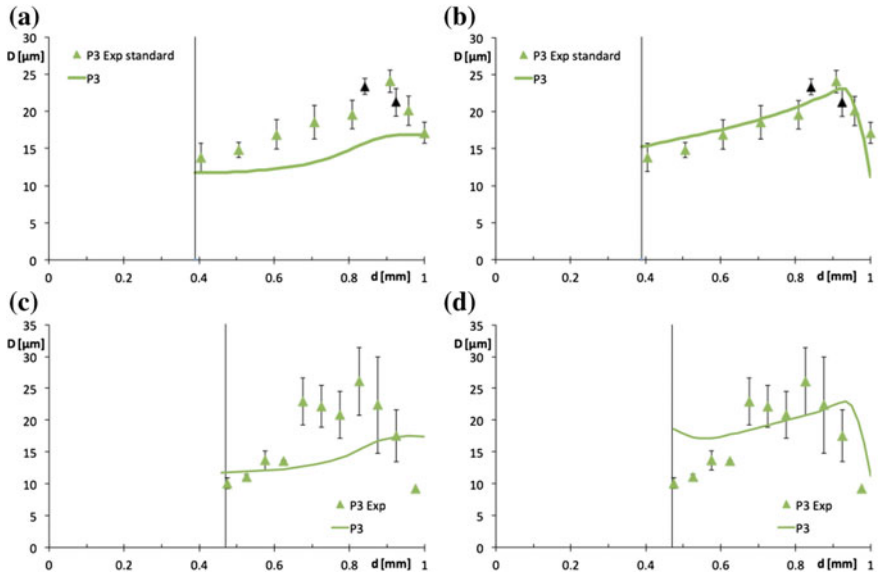

Fig. 5.29 Comparison of spherulite diameters, evaluated from AFM images both in "standard" and "slow" condition in position P3 along the flow path, with the predicted ones. In particular, for the "standard" condition predictions are obtained neglecting (**a**) and considering the FIC (**b**); for the "slow" condition, predictions are obtained neglecting (**c**) and considering the FIC (**d**). Data reproduced from [57]

phase and thus the formation of other nuclei is prevented giving rise to a larger spherulite diameters. A different correlation with a larger slope would give rise to a decrease of spherulites diameter by effect of FIC.

Second, closer to the midplane a decrease of diameters is correctly predicted when FIC is considered (the phenomenon is not reproduced when a quiescent crystallization kinetics is assumed). As stated above spherulite diameters increase by the effect of flow and approaching the midplane (where the effects of flow induced crystallization are lower) the diameters of the spherulites become smaller. Furthermore, the latent heat of crystallization keeps the region close to the sample midplane at higher temperatures and thus the crystallization at the midplane is delayed occurring at lower temperatures and thus giving rise to smaller spherulites (because the number of heterogeneous nuclei increases when the temperature decreases).

The mechanisms of formation of spherulitic and fibrillary layers are different. In particular, from experimental observation was found that fibrillary morphology develops when stretch and work are sufficiently high to form cylindrical rather spherical growth. As a consequence, predictions on the shear layer developed during the injection molding process can be obtained once a critical (shear rate) stretch value and a critical work value are identified. The thickness and the position of the shear layer are given by all the points presenting both calculated stretch parameter and viscous work higher than the chosen thresholds (critical values). By adopting this criterion, prediction of the shear layer position and thickness observed in the "standard" condition, can be obtained considering the calculated final distribution of the stretch parameter and viscous work reported in Fig. 5.30.

It can be noticed that, whatever realistic choice would be done for the two critical values, it would not sort a reasonable comparison with the thickness and the

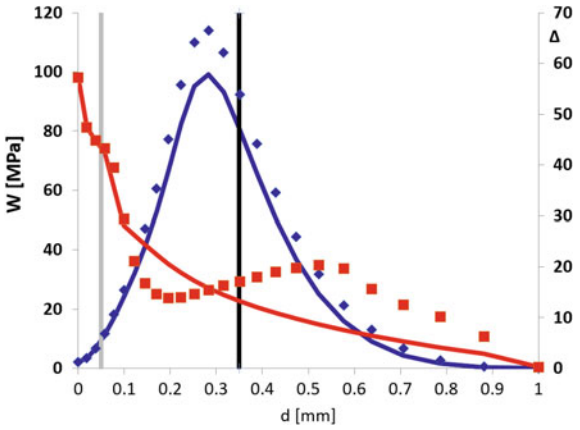

Fig. 5.30 Integral of the viscous work density (right axis) and molecular stretch parameter Δ (left axis), as function of the distance from the surface as calculated for the "standard" condition. The distribution of both variables at the end of the filling stage (lines) and at the end of the process (symbols) are reported. The thicknesses of the skin and shear layer are indicated as a vertical grey and black line respectively [73]

position of the skin and shear layers observed in the "standard" conditions. Similar conclusion was found for all the remaining conditions considered.

A realistic identification of the thicknesses and the position, within the molded samples cross sections, of the shear layers can be achieved by considering the following additional simultaneity criterion: the whole amount of work has to be done while the molecular stretch is above a critical value; furthermore, if the molecular stretch is let to relax below that critical value, all previous work has to be cancelled in the accounting for the critical work. This criterion appears physically grounded. In many processing conditions, the polymer melt is oriented first and then has the time to (partially) relax before being oriented again. If the relaxation were complete, it is obvious that the whole previous history does not have any effect of what happens next. This would mean that the time integral of the work alone is not a suitable criterion for describing the phenomenon in complex flow conditions and it is a sufficient condition whereas the integral of the viscous work and the final stretch distributions together can be considered a necessary criterion for fibrillar morphology of the polymer. The injection molding process seems specifically designed to verify the simultaneity criterion clarified above, since soon after filling the polymer not yet solidified relaxes considerable part of its stretch and after a short (but relevant) time it undergoes further stretching with lower shear rate but under higher viscosity due to the temperature decrease and eventually pressure increase. Furthermore, the *simultaneity* criterion is automatically respected in all the experiments conducted in literature that consider isothermal flow, under steady shear rate conditions.

In Fig. 5.31, the predictions of the position and thickness of the layers across the sample thickness, for all the conditions considered, are reported; results are obtained applying the *simultaneity* criterion and the same threshold values for

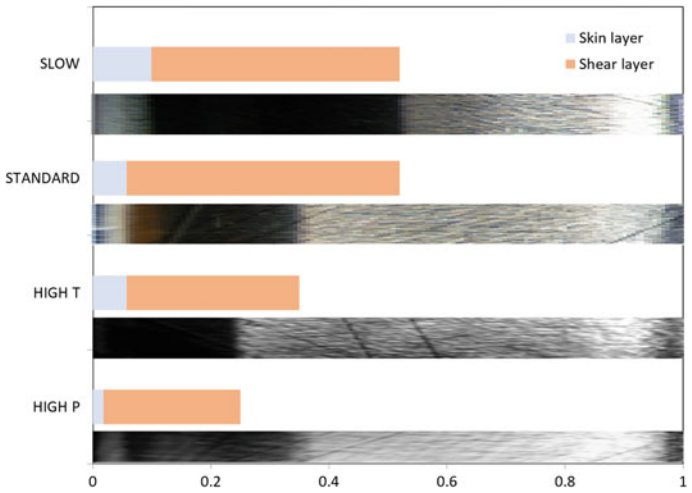

Fig. 5.31 Comparison between measured and predicted thickness and position of the layers across the sample thickness [73]

stretch parameter and critical work. The images of the samples are reported for a visual comparison of the results. It can be noticed that the thicknesses of the skin and of the shear layers are correctly described for all the samples molded with lower packing pressure (namely the standard, high T and slow conditions). An overestimation of the thickness of the shear layer for the sample molded with a pressure of 70 MPa (High P) is found. The reasons of this discrepancy can be found in the effect of pressure on viscosity (and on relaxation time) which obviously becomes extremely significant when the pressure levels increase.

5.6 Other Processing Techniques

5.6.1 Compression Molding

Compression molding is a process, commonly adopted for thermosets, in which the material, generally preheated, is first placed in an open, heated mold cavity. The mold is closed with a top force or plug member, pressure is applied to force the material into contact with all mold areas, while heat and pressure are maintained. Advanced PP composite can also be compression molded with unidirectional tapes, woven fabrics, randomly oriented fiber mat or chopped strand. The advantage of compression molding for thermoplastics is its ability to mold large, fairly intricate parts while injection molding could not be used. Therefore, the simplest way to produce isotropic plaques with different thicknesses is compression molding. Although crystallization occurs under a high pressure and temperature gradient, the melt flow and solid-state deformation are slight, so that the molded part possesses a relatively uniform texture (composed of spherulites). Transcrystals form sometimes at the mold surface. Compression-molded PP items are composed of spherulites and exhibit a random crystal orientation [112].

The lamellar thickness, spherulite size and crystallinity are the smaller, the larger the supercooling (defined as the difference between the melting point and crystallization temperature) is. High melting and cooling (mold) temperatures lead to a slow cooling and hence to a high crystallization temperature. This enhances both lamellar thickness spherulite size and crystallinity. The addition of nucleating agents increases the lamellar thickness and crystallinity and decreases the spherulite size. A high pressure has the same effect as the incorporation of nucleants [113].

While the tensile elongation decreases with increasing spherulite size, the yield strength and ultimate tensile strength scarcely depend on it. The tensile modulus, yield strength and hardness increase linearly with increasing crystallinity in contrast to the impact strength.

5.6.2 Extrusion-Related Techniques

Extruders (single screw or twin screw) are commonly used to produce tubes, profiles, films, and sheets, and to coat wires.

The geometry of a single screw extruder is usually constituted of a hopper which is used to feed the system with pellets (or sometimes with powder), a heated barrel (in fact successive zones with different controlled temperatures may be observed along the barrel), and a rotating screw whose core geometry generally increases from the hopper to the die.

For general extrusion of polypropylene, the temperature range from feed throat to front is 200–230 °C, with the die at the same temperature as the front barrel zone. Cast film, fibers, and yarns require higher temperatures; the rear at 220–250 °C and the front, adaptor, and die at 250 °C. Reverse profiles have been used where more mixing is required for pigment or fillers dispersion or melt uniformity.

Sheet and Pipe Extrusions

An extruded PP sheet shows a similar skin-core structure to that developed in injection molding. The skin layer is featureless and the core layer is composed of spherulites. The spherulite size increases toward the interior where the cooling is slower. A high draw ratio, creating high stresses, contributes to the initiation of crystal nuclei and thus to the formation of small spherulites [112]. The α crystallinity is low at the sheet surface and increases toward the interior. The α phase is almost replaced by the mesophase on the surface, with a slight intensification of the amorphous phase. A high draw ratio and short air gap, accompanied with a high melt orientation, initiates orientation crystallization and hence increases the crystallinity.

Film Casting

A cast film can be regarded as a thin sheet. While a sheet is composed mostly of the α-form crystals, in the case of the cast film, the cooling effect by the chill roll is so high that the α-crystals change gradually to the mesomorphic form. This modification is triggered by decreasing chill roll temperature. A PP with higher melt flow index (MFI) crystallizes more easily in the smectic form than a lower MFI resin. The spherulite size increases with increasing film thickness and chill roll temperature and decreases with increasing draw ratio and die temperature [114].

The molecular orientation increases with increasing draw ratio and take-up speed and with decreasing cylinder temperature. Crystallization during film casting is also the object of simulation work [115]. The tensile yield strength is higher and the ultimate elongation and strength are lower when the spherulite size becomes larger [114]. The tensile modulus increases linearly with increasing crystallinity. The heat sealing strength decreases with increase in the crystallinity.

Fiber Spinning

In melt spinning, the diameter of a filament extruded from a spinneret gradually decreases and approaches a constant value at the point of crystallization initiation (where crystallization and molecular orientation start). Because the melt-spun PP

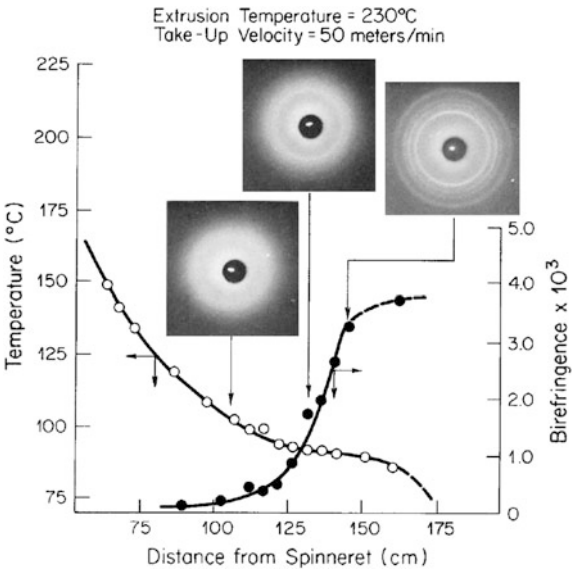

Fig. 5.32 On-line WAXS patterns, temperature and birefringence profiles for melt-spun polypropylene filament. Reproduced from [116]

fiber crystallizes under stresses, it is composed of a kind of shish-kebab structure [116].

Depending on the cooling rates, the spun filaments of polypropylene were either mesomorphic or highly crystalline. The mesomorphic form occurs only when rapid cooling rates were achieved by quenching the molten threadline into water.

For filaments spun into ambient air, crystallization to the α monoclinic form occurs in the threadline, as shown with on-line measurements in Fig. 5.32 [116]. The WAXD patterns made on a running filament at different distances from the spinneret are shown in relation to a temperature and birefringence profile for the same run. A hold in the temperature profile occurs as crystallization begins due to the release of the latent heat of crystallization. During crystallization the birefringence rises rapidly, eventually approaching the birefringence of the as-spun filament [116].

References

1. Natta G, Corradini P (1960) Structure and properties of isotactic polypropylene. Il Nuovo Cimento (1955–1965) 15(1):40–51. https://doi.org/10.1007/bf02731859
2. Coccorullo I, Pantani R, Titomanlio G (2003) Crystallization kinetics and solidified structure in iPP under high cooling rates. Polymer 44(1):307–318. https://doi.org/10.1016/S0032-3861(02)00762-0
3. Dorset D, McCourt M, Kopp S et al (1998) Isotactic polypropylene, β-phase: a study in frustration. Polymer 39(25):6331–6337. https://doi.org/10.1016/S0032-3861(97)10160-4

4. Angelloz C, Fulchiron R, Douillard A et al (2000) Crystallization of isotactic polypropylene under high pressure (γ phase). Macromolecules 33(11):4138–4145. https://doi.org/10.1021/ma991813e
5. De Rosa C, Auriemma F, Girolamo R et al (2014) Crystallization of the mesomorphic form and control of the molecular structure for tailoring the mechanical properties of isotactic polypropylene. J Polym Sci, Part B: Polym Phys 52(10):677–699. https://doi.org/10.1002/polb.23473
6. Varga J (2002) β-modification of isotactic polypropylene: preparation, structure, processing, properties, and application. J Macromol. Sci, Part B 41(4–6):1121–1171. https://doi.org/10.1081/MB-120013089
7. Lezak E, Bartczak Z, Galeski A (2006) Plastic deformation of the γ phase in isotactic polypropylene in plane-strain compression. Macromolecules 39(14):4811–4819. https://doi.org/10.1021/ma0605907
8. De Rosa C, Auriemma F, Di Girolamo R et al (2013) Morphology and mechanical properties of the mesomorphic form of isotactic polypropylene in stereodefective polypropylene. Macromolecules 46(13):5202–5214. https://doi.org/10.1021/ma400570k
9. Viana JC, Cunha A, Billon N (2001) The effect of the skin thickness and spherulite size on the mechanical properties of injection mouldings. J Mater Sci 36(18):4411–4418. https://doi.org/10.1023/A:1017970416968
10. Kristiansen M, Werner M, Tervoort T et al (2003) The binary system isotactic polypropylene/bis (3, 4-dimethylbenzylidene) sorbitol: phase behavior, nucleation, and optical properties. Macromolecules 36(14):5150–5156. https://doi.org/10.1021/ma030146t
11. Phillips AW, Bhatia A, Pw Zhu et al (2013) Polymorphism in sheared isotactic polypropylene containing nucleant particles. Macromol Mater Eng 298(9):991–1003. https://doi.org/10.1002/mame.201200199
12. Housmans J-W, Gahleitner M, Peters GW et al (2009) Structure–property relations in molded, nucleated isotactic polypropylene. Polymer 50(10):2304–2319. https://doi.org/10.1016/j.polymer.2009.02.050
13. Janeschitz-Kriegl H (2009) Crystallization modalities in polymer melt processing: fundamental aspects of structure formation. Springer Science & Business Media. https://doi.org/10.1007/978-3-211-87627-5
14. Piccarolo S, Saiu M, Brucato V et al. (1992) Crystallization of polymer melts under fast cooling. II. High-purity iPP. J Appl Polym Sci 46(4):625–634. https://doi.org/10.1002/app.1992.070460409
15. Magill J (1962) A new technique for following rapid rates of crystallization II isotactic polypropylene. Polymer 3:35–42. https://doi.org/10.1016/0032-3861(62)90064-2
16. Ding Z, Spruiell JE (1996) An experimental method for studying nonisothermal crystallization of polymers at very high cooling rates. J Polym Sci, Part B: Polym Phys 34(16):2783–2804. https://doi.org/10.1002/(SICI)1099-0488(19961130)34:16%3c2783:AID-POLB12%3e3.0.CO;2-6
17. Brucato V, De Santis F, Giannattasio A et al (2002) Crystallization during fast cooling experiments, a novel apparatus for real time monitoring. Macromol Symp 185:181–196. https://doi.org/10.1002/1521-3900(200208)185:1%3c181:AID-MASY181%3e3.0.CO;2-O
18. De Santis F, Lamberti G, Peters GW et al (2005) Improved experimental characterization of crystallization kinetics. Eur Polymer J 41(10):2297–2302. https://doi.org/10.1016/j.eurpolymj.2005.04.032
19. Adamovsky S, Schick C (2004) Ultra-fast isothermal calorimetry using thin film sensors. Thermochim Acta 415(1–2):1–7. https://doi.org/10.1016/j.tca.2003.07.015
20. De Santis F, Adamovsky S, Titomanlio G et al (2006) Scanning nanocalorimetry at high cooling rate of isotactic polypropylene. Macromolecules 39(7):2562–2567. https://doi.org/10.1021/ma052525n
21. De Santis F, Adamovsky S, Titomanlio G et al (2007) Isothermal nanocalorimetry of isotactic polypropylene. Macromolecules 40(25):9026–9031. https://doi.org/10.1021/ma071491b

22. Morrow D, Newman B (1968) Crystallization of low-molecular-weight polypropylene fractions. J Appl Phys 39(11):4944–4950. https://doi.org/10.1063/1.1655891
23. Turner-Jones A (1971) Development of the γ-crystal form in random copolymers of propylene and their analysis by DSC and X-ray methods. Polymer 12(8):487–508. https://doi.org/10.1016/0032-3861(71)90031-0
24. Mezghani K, Phillips PJ (1995) γ-Phase in propylene copolymers at atmospheric pressure. Polymer 36(12):2407–2411. https://doi.org/10.1016/0032-3861(95)97341-C
25. Meille SV, Bruckner S, Porzio W (1990) γ-Isotactic polypropylene. A structure with nonparallel chain axes. Macromolecules 23(18):4114–4121. https://doi.org/10.1021/ma00220a014
26. Sauer J, Pae K (1968) Structure and Thermal Behavior of Pressure-Crystallized Polypropylene. J Appl Phys 39(11):4959–4968. https://doi.org/10.1063/1.1655893
27. Nakafuku C (1981) High pressure dta study on the melting and crystallization of isotactic polypropylene. Polymer 22(12):1673–1676. https://doi.org/10.1016/0032-3861(81)90384-0
28. Campbell RA, Phillips PJ, Lin J (1993) The gamma phase of high-molecular-weight polypropylene: 1. Morphological aspects. Polymer 34(23):4809–4816. https://doi.org/10.1016/0032-3861(93)90002-R
29. Meille SV, Brückner S (1989) Non-parallel chains in crystalline γ-isotactic polypropylene. Nature 340(6233):455–457. https://doi.org/10.1038/340455a0
30. Zoller P, Bolli P, Pahud V et al (1976) Apparatus for measuring pressure–volume–temperature relationships of polymers to 350 C and 2200 kg/cm2. Rev Sci Instrum 47 (8):948–952. https://doi.org/10.1063/1.1134779
31. Zoller P (1979) Pressure–volume–temperature relationships of solid and molten polypropylene and poly (butene-1). J Appl Polym Sci 23(4):1057–1061. https://doi.org/10.1002/app.1979.070230411
32. He J, Zoller P (1994) Crystallization of polypropylene, nylon-66 and poly (ethylene terephthalate) at pressures to 200 MPa: Kinetics and characterization of products. J Polym Sci, Part B: Polym Phys 32(6):1049–1067. https://doi.org/10.1002/polb.1994.090320610
33. La Carrubba V, Brucato V, Piccarolo S (2002) Phenomenological approach to compare the crystallization kinetics of isotactic polypropylene and polyamide-6 under pressure. J Polym Sci, Part B: Polym Phys 40(1):153–175. https://doi.org/10.1002/polb.10075
34. Pantani R, Nappo V, De Santis F et al (2014) Fibrillar Morphology in Shear-Induced Crystallization of Polypropylene. Macromol Mater Eng 299(12):1465–1473. https://doi.org/10.1002/mame.201400131
35. van Erp TB, Balzano L, Spoelstra AB et al (2012) Quantification of non-isothermal, multi-phase crystallization of isotactic polypropylene: The influence of shear and pressure. Polymer 53(25):5896–5908. https://doi.org/10.1016/j.polymer.2012.10.027
36. De Santis F, Pantani R, Titomanlio G (2016) Effect of shear flow on spherulitic growth and nucleation rates of polypropylene. Polymer 90:102–110. https://doi.org/10.1016/j.polymer.2016.02.059
37. Pantani R, Coccorullo I, Volpe V et al (2010) Shear-induced nucleation and growth in isotactic polypropylene. Macromolecules 43(21):9030–9038. https://doi.org/10.1021/ma101775h
38. Pantani R, Nappo V, De Santis F et al (2014) Fibrillar morphology formation in a sheared polypropylene melt. AIP Conf Proc 1593:76–79. https://doi.org/10.1063/1.4873738
39. Janeschitz-Kriegl H, Ratajski E, Stadlbauer M (2003) Flow as an effective promotor of nucleation in polymer melts: a quantitative evaluation. Rheol Acta 42(4):355–364. https://doi.org/10.1007/s00397-002-0247-x
40. Mykhaylyk OO, Chambon P, Graham RS et al (2008) The specific work of flow as a criterion for orientation in polymer crystallization. Macromolecules 41(6):1901–1904. https://doi.org/10.1021/ma702603v
41. Troisi E, Arntz S, Roozemond P et al (2017) Application of a multi-phase multi-morphology crystallization model to isotactic polypropylenes with different molecular weight distributions. Eur Polymer J 97:397–408. https://doi.org/10.1016/j.eurpolymj.2017.09.042

42. van Erp TB, Balzano L, Peters GW (2012) Oriented gamma phase in isotactic polypropylene homopolymer. ACS Macro Letters 1(5):618–622. https://doi.org/10.1021/mz3000978
43. Gahleitner M, Mileva D, Androsch R et al (2016) Crystallinity-based product design: Utilizing the polymorphism of isotactic PP homo-and copolymers. Int Polym Proc 31 (5):618–627. https://doi.org/10.3139/217.3242
44. Menyhárd A, Gahleitner M, Varga J et al (2009) The influence of nucleus density on optical properties in nucleated isotactic polypropylene. Eur Polymer J 45(11):3138–3148. https://doi.org/10.1016/j.eurpolymj.2009.08.006
45. Libster D, Aserin A, Garti N (2007) Advanced nucleating agents for polypropylene. Polym Adv Technol 18(9):685–695. https://doi.org/10.1002/pat.970
46. Karger-Kocsis J, Varga J, Ehrenstein G (1997) Comparison of the fracture and failure behavior of injection-molded α-and β-polypropylene in high-speed three-point bending tests. J Appl Polym Sci 64(11):2057–2066. https://doi.org/10.1002/(SICI)1097-4628(19970613)64:11%3c2057:AID-APP1%3e3.0.CO;2-I
47. Yoshimoto S, Ueda T, Yamanaka K et al (2001) Epitaxial act of sodium 2, 2′-methylene-bis-(4, 6-di-t-butylphenylene) phosphate on isotactic polypropylene. Polymer 42(23):9627–9631. https://doi.org/10.1016/S0032-3861(01)00510-9
48. Liu H, Huo H (2013) Competitive growth of α-and β-crystals in isotactic polypropylene with versatile nucleating agents under shear flow. Colloid Polym Sci 291(8):1913–1925. https://doi.org/10.1007/s00396-013-2922-0
49. Menyhárd A, Varga J, Molnár G (2006) Comparison of different-nucleators for isotactic polypropylene, characterisation by DSC and temperature-modulated DSC (TMDSC) measurements. J Therm Anal Calorim 83(3):625–630. https://doi.org/10.1007/s10973-005-7498-6
50. Výchopňová J, Habrová V, Obadal M et al (2006) Crystallization of polypropylenewith a minute amount of β-nucleator. J Therm Anal Calorim 86(3):687–691. https://doi.org/10.1007/s10973-006-7894-6
51. Libster D, Aserin A, Garti N (2006) A novel dispersion method comprising a nucleating agent solubilized in a microemulsion, in polymeric matrix: II. Microemulsion characterization. J. colloid interface sci 302 (1):322–329. https://doi.org/10.1016/j.jcis.2006.06.060
52. Fillon B, Lotz B, Thierry A et al. (1993) Self-nucleation and enhanced nucleation of polymers. Definition of a convenient calorimetric "efficiency scale" and evaluation of nucleating additives in isotactic polypropylene (α phase). J Polym Sci Part B: Polym Phys 31 10):1395–1405. https://doi.org/10.1002/polb.1993.090311014
53. Nagasawa S, Fujimori A, Masuko T et al (2005) Crystallisation of polypropylene containing nucleators. Polymer 46(14):5241–5250. https://doi.org/10.1016/j.polymer.2005.03.099
54. Pantani R, Coccorullo I, Speranza V et al (2005) Modeling of morphology evolution in the injection molding process of thermoplastic polymers. Prog Polym Sci 30(12):1185–1222. https://doi.org/10.1016/j.progpolymsci.2005.09.001
55. Isayev A, Catignani B (1997) Crystallization and microstructure in quenched slabs of various molecular weight polypropylenes. Polym Eng Sci 37(9):1526–1539. https://doi.org/10.1002/pen.11801
56. Eder G, Janeschitz-Kriegl H, Liedauer S (1990) Crystallization processes in quiescent and moving polymer melts under heat transfer conditions. Prog Polym Sci 15(4):629–714. https://doi.org/10.1016/0079-6700(90)90008-O
57. Pantani R, Speranza V, Titomanlio G (2017) Effect of Flow-Induced Crystallization on the distribution of spherulite dimensions along cross section of injection molded parts. Eur Polymer J 97:220–229. https://doi.org/10.1016/j.eurpolymj.2017.10.012
58. Hoffman JD, Lauritzen J (1961) Crystallization of bulk polymers with chain folding-Theory of growth of lamellar spherulites. J Res National Bureau Standards 4:297–336. https://doi.org/10.6028/jres.065A.035
59. Hoffman J, Lauritzen J, Passaglia E et al (1969) Kinetics of polymer crystallization from solution and the melt. Kolloid-Zeitschrift und Zeitschrift für Polymere 231(1–2):564–592. https://doi.org/10.1007/BF01500015

60. Roozemond PC, van Drongelen M, Peters GW (2016) Modeling flow-induced crystallization. In: Auriemma F. AG, de Rosa C (ed) Polymer Crystallization II. Springer, pp 243–294. https://doi.org/10.1007/12_2016_35
61. Karger-Kocsis J, Csikai I (1987) Skin-core morphology and failure of injection-molded specimens of impact-modified polypropylene blends. Polym Eng Sci 27(4):241–253. https://doi.org/10.1002/pen.760270403
62. Balzano L, Rastogi S, Peters GW (2008) Flow induced crystallization in isotactic polypropylene − 1, 3: 2, 4-bis (3, 4-dimethylbenzylidene) sorbitol blends: implications on morphology of shear and phase separation. Macromolecules 41(2):399–408. https://doi.org/10.1021/ma071460g
63. Laschet G, Spekowius M, Spina R et al (2017) Multiscale simulation to predict microstructure dependent effective elastic properties of an injection molded polypropylene component. Mech Mater 105:123–137. https://doi.org/10.1016/j.mechmat.2016.10.009
64. Liu F, Guo C, Wu X et al (2012) Morphological comparison of isotactic polypropylene parts prepared by micro-injection molding and conventional injection molding. Polym Adv Technol 23(3):686–694. https://doi.org/10.1002/pat.1946
65. Giboz J, Copponnex T, Mélé P (2009) Microinjection molding of thermoplastic polymers: morphological comparison with conventional injection molding. J Micromech Microeng 19 (2):025023. https://doi.org/10.1088/0960-1317/19/2/025023
66. Giboz J, Spoelstra AB, Portale G et al (2011) On the origin of the "core-free" morphology in microinjection-molded HDPE. J Polym Sci, Part B: Polym Phys 49(20):1470–1478. https://doi.org/10.1002/polb.22332
67. Wang S, Wang Z, Zhao N et al (2015) A novel morphology development of micro-injection molded isotactic polypropylene. RSC Advances 5(52):41608–41610. https://doi.org/10.1039/C5RA04626B
68. Jerschow P, Janeschitz-Kriegl H (1996) On the development of oblong particles as precursors for polymer crystallization from shear flow: origin of the so-called fine grained layers. Rheol Acta 35(2):127–133. https://doi.org/10.1007/BF00396039
69. Liparoti S, Speranza V, Sorrentino A et al (2017) Mechanical properties distribution within polypropylene injection molded samples: effect of mold temperature under uneven thermal conditions. Polymers 9(11):585. https://doi.org/10.3390/polym9110585
70. Kantz M, Newman H, Stigale F (1972) The skin-core morphology and structure–property relationships in injection-molded polypropylene. J Appl Polym Sci 16(5):1249–1260. https://doi.org/10.1002/app.1972.070160516
71. Kalay G, Bevis MJ (1997) Processing and physical property relationships in injection-molded isotactic polypropylene. 2. Morphology and crystallinity. J Polym Sci Part B: Polym Phys 35(2):265–291. https://doi.org/10.1002/(sici)1099-0488(19970130)35:2%3c265::aid-polb6%3e3.0.co;2-r
72. Mi D, Xia C, Jin M et al (2016) Quantification of the effect of shish-kebab structure on the mechanical properties of polypropylene samples by controlling shear layer thickness. Macromolecules 49(12):4571–4578. https://doi.org/10.1021/acs.macromol.6b00822
73. Pantani R, Speranza V, Titomanlio G (2018) A criterion for the formation of fibrillar layers in injection molded parts. Int Polym Process. in press
74. Speranza V, Vietri U, Pantani R (2011) Monitoring of injection molding of thermoplastics: Average solidification pressure as a key parameter for quality control. Macromol Res 19 (6):542. https://doi.org/10.1007/s13233-011-0610-9
75. Tosello G, Hansen HN (2010) Micro injection molding. In: Micro-manufacturing engineering and technology. Elsevier Science, pp 90–113. https://doi.org/10.1016/b978-0-323-31149-6.00009-8
76. Ito H, Yagisawa Y, SAITO T et al (2005) Fundamental study on structure development of thin-wall injection molded products. Theor Appl Mech Jpn 54:263–268. https://doi.org/10.11345/nctam.54.263

77. De Santis F, Pantani R (2016) Development of a rapid surface temperature variation system and application to micro-injection molding. J Mater Process Technol 237:1–11. https://doi.org/10.1016/j.jmatprotec.2016.05.023
78. Speranza V, Liparoti S, Calaon M et al (2017) Replication of micro and nano-features on iPP by injection molding with fast cavity surface temperature evolution. Mater Des 133:559–569. https://doi.org/10.1016/j.matdes.2017.08.016
79. Liparoti S, Titomanlio G, Sorrentino A (2016) Analysis of asymmetric morphology evolutions in iPP molded samples induced by uneven temperature field. AIChE J 62 (8):2699–2712. https://doi.org/10.1002/aic.15241
80. Wang G, Zhao G, Wang X (2014) Development and evaluation of a new rapid mold heating and cooling method for rapid heat cycle molding. Int J Heat Mass Transf 78:99–111. https://doi.org/10.1016/j.ijheatmasstransfer.2014.06.062
81. Kmetty Á, Bárány T, Karger-Kocsis J (2010) Self-reinforced polymeric materials: a review. Prog Polym Sci 35(10):1288–1310
82. Allan P, Bevis M (1987) Multiple live-feed injection moulding. Plastics and rubber processing and applications 7(1):3–10
83. Kalay G, Allan P, Bevis MJ (1994) γ Phase in injection moulded isotactic polypropylene. Polymer 35(12):2480–2482. https://doi.org/10.1016/0032-3861(94)90366-2
84. Kalay G, Bevis MJ (1997) Processing and physical property relationships in injection-molded isotactic polypropylene. 1. Mechanical properties. J Polym Sci Part B: Polym Phys 35(2):241–263. https://doi.org/10.1002/(sici)1099-0488(19970130)35:2%3c241::aid-polb5%3e3.0.co;2-v
85. Lei J, Jiang C, Shen K (2004) Biaxially self-reinforced high-density polyethylene prepared by dynamic packing injection molding. I. Processing parameters and mechanical properties. J Appl polym Sci 93(4):1584–1590
86. Guan Q, Zhu X, Chiu D et al (1996) Self-reinforcement of polypropylene by oscillating packing injection molding under low pressure. J Appl Polym Sci 62(5):755–762. https://doi.org/10.1002/(SICI)1097-4628(19961031)62:5%3c755:AID-APP6%3e3.0.CO;2-V
87. Chen LM, Shen K (2000) Biaxial self-reinforcement of isotactic polypropylene prepared in uniaxial oscillating stress field by injection molding. I. Processing conditions and mechanical properties. J Appl Polym Sci 78(11):1906–1910. https://doi.org/10.1002/1097-4628(20001209)78:11%3c1906::aid-app80%3e3.0.co;2-l
88. Wang Y, Pan J-L, Mao Y et al (2010) Spatial distribution of γ-crystals in metallocene-made isotactic polypropylene crystallized under combined thermal and flow fields. J Phys Chem B 114(20):6806–6816. https://doi.org/10.1021/jp1002484
89. Chen Y-H, Zhong G-J, Wang Y et al (2009) Unusual tuning of mechanical properties of isotactic polypropylene using counteraction of shear flow and β-nucleating agent on β-form nucleation. Macromolecules 42(12):4343–4348. https://doi.org/10.1021/ma900411f
90. Su R, Zhang Z, Gao X et al (2010) Polypropylene injection molded part with novel macroscopic bamboo-like bionic structure. J Phys Chem B 114(31):9994–10001. https://doi.org/10.1021/jp1020802
91. Sato A, Ito H, Koyama K (2009) Study of application of ultrasonic wave to injection molding. Polym Eng Sci 49(4):768–773. https://doi.org/10.1002/pen.21268
92. Peng B, Wu H, Guo S et al (2007) Effects of ultrasonic oscillations on rheological behavior and mechanical properties of novel propylene-based plastomers. J Appl Polym Sci 106 (3):1725–1732. https://doi.org/10.1002/app.26765
93. Ibar J (1998) Control of polymer properties by melt vibration technology: a review. Polym Eng Sci 38(1):1–20. https://doi.org/10.1002/pen.10161
94. Li Y, Shen K (2008) Improving the mechanical properties of polypropylene via melt vibration. J Appl Polym Sci 109(1):90–96. https://doi.org/10.1002/app.27412
95. Youbing L, Jing C, Kaizhi S (2008) Self-reinforced isotactic polypropylene prepared by melt vibration injection molding. Polym Plast Technol Eng 47(7):673–677. https://doi.org/10.1080/03602550802129551

96. Liu K, Zhang J, Liu H et al. (2013) A multi-layer bioinspired design with evolution of shish-kebab structures induced by controlled periodical shear field. Express Polym Lett 7(4). https://doi.org/10.3144/expresspolymlett.2013.32
97. Guo X, Isayev A, Guo L (1999) Crystallinity and microstructure in injection moldings of isotactic polypropylenes. Part 1: A new approach to modeling and model parameters. Polym Eng Sci 39(10):2096–2114. https://doi.org/10.1002/pen.11601
98. Guo X, Isayev A, Demiray M (1999) Crystallinity and microstructure in injection moldings of isotactic polypropylenes. Part II: Simulation and experiment. Polym Eng Sci 39 (11):2132–2149. https://doi.org/10.1002/pen.11603
99. Zuidema H, Peters GW, Meijer HE (2001) Development and validation of a recoverable strain-based model for flow-induced crystallization of polymers. Macromol Theory Simul 10 (5):447–460. https://doi.org/10.1002/1521-3919(20010601)10:5%3c447:AID-MATS447%3e3.0.CO;2-C
100. Eder G, Janeschitz-Kriegl H (1997) Crystallization. In: Meijer H (ed) Materials science and technology: processing of polymers, vol 18. Wiley-VCH. https://doi.org/10.1002/9783527603978.mst0211
101. Baaijens F (1991) Calculation of residual stresses in injection molded products. Rheol Acta 30(3):284–299. https://doi.org/10.1007/BF00366642
102. Leonov A (1987) On a class of constitutive equations for viscoelastic liquids. J Nonnewton Fluid Mech 25(1):1–59. https://doi.org/10.1016/0377-0257(87)85012-7
103. Zheng R, Kennedy P (2004) A model for post-flow induced crystallization: General equations and predictions. J Rheol 48(4):823–842. https://doi.org/10.1122/1.1763944
104. Mykhaylyk OO, Chambon P, Impradice C et al (2010) Control of structural morphology in shear-induced crystallization of polymers. Macromolecules 43(5):2389–2405. https://doi.org/10.1021/ma902495z
105. Gahleitner M, Wolfschwenger J, Bachner C et al (1996) Crystallinity and mechanical properties of PP-homopolymers as influenced by molecular structure and nucleation. J Appl Polym Sci 61(4):649–657. https://doi.org/10.1002/(SICI)1097-4628(19960725)61:4%3c649:AID-APP8%3e3.0.CO;2-L
106. Salazar A, Rico A, Rodriguez S et al (2012) Relating fracture behavior to spherulite size in conrolled-rheology polypropylenes. Polym Eng Sci 52(4):805–813. https://doi.org/10.1002/pen.22145
107. Pantani R, Sorrentino A, Speranza V et al (2004) Molecular orientation in injection molding: experiments and analysis. Rheol Acta 43(2):109–118. https://doi.org/10.1007/s00397-003-0325-8
108. Pantani R, Speranza V, Titomanlio G (2016) Thirty years of modeling of injection molding. a brief review of the contribution of UNISA code to the field. Int Polym Process 31(5):655–663. https://doi.org/10.3139/217.3249
109. Titomanlio G, Speranza V, Brucato V (1997) On the simulation of thermoplastic injection moulding process: II relevance of interaction between flow and crystallization. Int Polym Proc 12(1):45–53. https://doi.org/10.3139/217.970045
110. Pantani R, Speranza V, Titomanlio G (2001) Relevance of mold-induced thermal boundary conditions and cavity deformation in the simulation of injection molding. Polym Eng Sci 41 (11):2022–2035. https://doi.org/10.1002/pen.10898
111. Pantani R, De Meo A, Speranza V et al (2015) Effect of crystallinity on the viscosity of an isotactic polypropylene. AIP Conf Proc 1695:020065. https://doi.org/10.1063/1.4873738
112. Karger-Kocsis J (2012) Polypropylene: an AZ reference, vol 2. Springer Science & Business Media. https://doi.org/10.1007/978-94-011-4421-6
113. Reinshagen J, Dunlap R (1975) The effects of melt history, crystallization pressure, and crystallization temperature on the crystallization and resultant structure of bulk isotactic polypropylene. J Appl Polym Sci 19(4):1037–1060. https://doi.org/10.1002/app.1975.070190413

114. Akay M (1989) Influence of total processing history on polypropylene structure and properties. Polym Int 21(4):285–293. https://doi.org/10.1002/pi.4980210402
115. Titomanlio G, Lamberti G (2004) Modeling flow induced crystallization in film casting of polypropylene. Rheol Acta 43(2):146–158. https://doi.org/10.1007/s00397-003-0329-4
116. Nadella HP, Henson HM, Spruiell JE et al (1977) Melt spinning of isotactic polypropylene: Structure development and relationship to mechanical properties. J Appl Polym Sci 21 (11):3003–3022. https://doi.org/10.1002/app.1977.070211115